Scattering and Neutrino Detector at the LHC

Letter of Intent

SND Collaboration

CERN-LHCC-2020-013 / LHCC-I-037
27/08/2020

Abstract

We propose to build and operate a detector that will, for the first time, measure the process $pp \to \nu X$ at the LHC and search for feebly interacting particles (FIPs) in an unexplored domain. The TI18 tunnel has been identified as a suitable site to perform these measurements due to very low machine-induced background. The detector will be off-axis with respect to the ATLAS interaction point (IP1) and, given the pseudo-rapidity range accessible, the corresponding neutrinos will mostly come from charm decays: the proposed experiment will thus make the first test of the heavy flavour production in a pseudo-rapidity range that is not accessible to the current LHC detectors. In order to efficiently reconstruct neutrino interactions and identify their flavour, the detector will combine in the target region nuclear emulsion technology with scintillating fibre tracking layers and it will adopt a muon identification system based on scintillating bars that will also play the role of a hadronic calorimeter. A time of flight measurement will also be achieved thanks to a dedicated timing detector. The operation of this detector will provide an important test of neutrino reconstruction in a high occupancy environment in view of a possible experiment at HL-LHC or at the SPS Beam Dump Facility.

C. Ahdida[24], R. Albanese[9,c,g], A. Alexandrov[9,19,21,c], M. Andreini[24], A. Anokhina[22], A. Bay[25], P. Bestmann[24], C. Betancourt[26], I. Bezshyiko[26], A. Blanco[33],M. Bogomilov[1], K. Bondarenko[24,25], W.M. Bonivento[8], A. Boyarsky[18,d], L.R. Buonocore[26], A. Buonaura[26], S. Buontempo[9], T. Camporesi[24], M. Campanelli[30], V. Canale[9,c], F. Cerutti[24], N. Charitonidis[24], M. Chernyavskiy[19], K.-Y. Choi[17], S. Cholak[25], V. Cicero[7], L. Congedo[6,a], M. Cristinziani[4], A. Crupano[9,c], G.M. Dallavalle[7], A. Datwyler[26], N. D'Ambrosio[10], A. Dashkina[21], R. de Asmundis[9,c], J. De Carvalho Saraiva[33], P.T. De Bryas Dexmiers D'Archiac[25], G. De Lellis[9,21,c], M. de Magistris[9,c], A. De Roeck[24], A. De Rujula[31], M. De Serio[6,a], D. De Simone[26], L. Dedenko[22], A. Di Crescenzo[9,c], L. Di Giulio[24], A. Dolmatov[20], O. Durhan[27], D. Fasanella[7], F. Fedotovs[29], M. Ferrillo[26], M. Ferro-Luzzi[24], R.A. Fini[6], P. Fonte[33],C. Franco[33],R. Fresa[9,c], G. Galati[9,c], J. Gall[24], V. Gentile[9,21,c], A. Golovatiuk[9,c], A. Golutvin[29,21], P. Gorbounov[24], M. Gorshenkov[21], E. Graverini[25], J.-L. Grenard[24], A.M. Guler[27], G.J. Haefeli[25], E.van Herwijnen[21], B. Hosseini[29], G. Iaselli[6,a], P. Iengo[9,24], S. Ilieva[1] A. Iuliano[9,c], R. Jacobsson[24], M. Jonker[24], C. Kamiscioglu[27,f], Y. Karyotakis[32], E. Khalikov[22], Y.G. Kim[14], J.W. Ko[13], D.I. Kolev[1], M. Komatsu[11], N. Konovalova[19,21], I. Krasilnikova[21], H.M. Lacker[1], O. Lantwin[26,21], A. Lauria[9,c], K.S. Lee[16], K.Y. Lee[13], S. Lo Meo[7,b], V.P. Loschiavo[9,g], L. Lopes[33], A. Magnan[29], A. Malinin[20], A.K. Managadze[22], S. Marsh[24], A. Miano[9,c], A. Montanari[7], M.C. Montesi[9,c], T. Naka[12], F.L. Navarria[7], P. Ninin[24], S. Ogawa[12], N. Okateva[19,21], J. Osborne[24], N. Owtscharenko[4], P.H. Owen[26], B.D. Park[13], G. Passeggio[9], A. Pastore[6], M. Patel[29,21], L. Patrizii[7,b], A. Pertrov[20], D. Podgrudkov[22], G.L. Petkov[1], K. Petridis[28], N. Polukhina[19,21,e], A. Prota[9,c], A. Quercia[9,c], F. Ratnikov[23], F. Redi[25], A.B. Rodrigues Cavalcante[25], T. Roganova[22], T. Rovelli[7,b], O. Ruchayskiy[2], T. Ruf[24], M. Sabate Gilarte[24], F. Sanchez Galan[24], P. Santos Diaz[24], O. Schneider[25], G. Sekhniaidze[9], N. Serra[26,21], M. Shaposhnikov[25], T. Shchedrina[19,21], L. Shchutska[25], V. Shevchenko[20,21], H. Shibuya[12], S. Shirobokov[29], E. Shmanin[21], S. Simone[6,a], G. Sirri[7,b], J.Y. Sohn[13], N. Starkov[19,21], J.L. Tastet[2], I. Timiryasov[25], V. Tioukov[9], N. Tosi[7,b], F. Tramontano[9,c], R. Tsenov[1], E. Ursov[22], A. Ustyuzhanin[23,21], G. Vankova-Kirilova[1], C. Vendeuvre[24], C. Visone[9,c], R. Wanke[5], J.-K. Woo[15], C.S. Yoon[13], E. Zaffaroni[25]

[1] *Faculty of Physics, Sofia University, Sofia, Bulgaria*
[2] *Niels Bohr Institute, University of Copenhagen, Copenhagen, Denmark*
[3] *Humboldt-Universität zu Berlin, Berlin, Germany*
[4] *Physikalisches Institut, Universität Bonn, Bonn, Germany*
[5] *Institut für Physik and PRISMA Cluster of Excellence, Johannes Gutenberg Universität Mainz, Mainz, Germany*
[6] *Sezione INFN di Bari, Bari, Italy*
[7] *Sezione INFN di Bologna, Bologna, Italy*
[8] *Sezione INFN di Cagliari, Cagliari, Italy*
[9] *Sezione INFN di Napoli, Napoli, Italy*
[10] *Laboratori Nazionali dell'INFN di Gran Sasso, L'Aquila, Italy*
[11] *Nagoya University, Nagoya, Japan*
[12] *Toho University, Funabashi, Chiba, Japan*
[13] *Physics Education Department & RINS, Gyeongsang National University, Jinju, Korea*
[14] *Gwangju National University of Education, Gwangju, Korea*
[15] *Jeju National University, Jeju, Korea*
[16] *Korea University, Seoul, Korea*

[17] *Sungkyunkwan University, Suwon-si, Gyeong Gi-do, Korea*
[18] *University of Leiden, Leiden, The Netherlands*
[19] *P.N. Lebedev Physical Institute (LPI RAS), Moscow, Russia*
[20] *National Research Centre 'Kurchatov Institute', Moscow, Russia*
[21] *National University of Science and Technology 'MISiS', Moscow, Russia*
[22] *Skobeltsyn Institute of Nuclear Physics of Moscow State University (SINP MSU), Moscow, Russia*
[23] *National Research University Higher School of Economics, Moscow, Russia*
[24] *European Organization for Nuclear Research (CERN), Geneva, Switzerland*
[25] *École Polytechnique Fédérale de Lausanne (EPFL), Lausanne, Switzerland*
[26] *Physik-Institut, Universität Zürich, Zürich, Switzerland*
[27] *Middle East Technical University (METU), Ankara, Turkey*
[28] *H.H. Wills Physics Laboratory, University of Bristol, Bristol, United Kingdom*
[29] *Imperial College London, London, United Kingdom*
[30] *University College London, London, United Kingdom*
[31] *Inst. de Estructura de la Materia, Consejo Superior de Investigaciones Cientificas (CSIC), Madrid, Spain*
[32] *Laboratoire d'Annecy-le-Vieux de Physique des Particules (LAPP), Annecy-le-Vieux, France*
[33] *LIP, Laboratory of Instrumentation and Experimental Particle Physics, Portugal*
[a] *Università di Bari, Bari, Italy*
[b] *Università di Bologna, Bologna, Italy*
[c] *Università di Napoli "Federico II", Napoli, Italy*
[d] *Taras Shevchenko National University of Kyiv, Kyiv, Ukraine*
[e] *National Research Nuclear University (MEPhI), Moscow, Russia*
[f] *Ankara University, Ankara, Turkey*
[g] *Consorzio CREATE, Napoli, Italy*

1 Physics motivation

The Standard Model of particle physics (SM) has been able to describe all known microscopic physics phenomena with great precision. However, as well known, there are several failures of the SM of cosmological and astrophysical origin, such as the existence of Dark Matter (DM) and the baryon-antibaryon asymmetry in the Universe, along with neutrino masses and oscillations that also require some physics beyond the Standard Model.

To date no firm signs of new physics that would provide resolution to these puzzles have been discovered at the LHC and other particle physics experiments. Recently, measurements from LHCb and B-factories have shown a set of discrepancies with respect to SM predictions (see e.g. [1, 2, 3]). While it is not clear yet if these measurements are statistical fluctuations or a genuine sign of new physics, experiment, such as ATLAS, CMS, LHCb and Belle, will continue to test them in a canonical way. It is therefore important to perform complementary measurements. Below we describe how to test lepton flavor universality in the neutrino sector.

The neutrino sector allows precise tests of the SM [4, 5, 6, 7] and a probe for new physics [8, 9], in an otherwise veiled region of the Universe [10]. Neutrino interactions have been measured in the energy regime below 350 GeV, and recently, the IceCube collaboration reported a few tens of events in the region 10 TeV-1 PeV [11]. It is notable that the region between 350 GeV and 10 TeV is currently unexplored. Measurements of neutrino interactions in the last decades were mainly performed at energies where neutrino oscillations are enhanced over available baselines. In addition, there are basically no electron neutrino measurements above 10 GeV. Concerning tau neutrinos, only an handful of events observed by the DONUT [12] and OPERA [13, 14] experiments have been recorded. The DONUT experiment at Fermilab performed the first observation of tau neutrinos using a 800 GeV proton beam dump on to a tungsten target. The experiment observed the first nine tau neutrino candidates [12], without distinguishing between neutrinos and anti-neutrinos and did not study interactions of other neutrino types. OPERA observed ten tau neutrino candidates coming from muon neutrino oscillations and also detected 35 electron neutrino interactions [15]. The emulsion technology developed by OPERA proved to be capable of identifying the three neutrino flavours.

Recently, a beam dump facility has been designed to host the SHiP experiment [16], searching for hidden particles and studying neutrino physics [17]. Beam dump facilities provide an intense flux of neutrinos when using a correspondingly intense proton beam. If protons have sufficient energy, the neutrino beam includes also tau neutrinos. This is the case for SHiP where, in about a decade from now, 2×10^{20} protons from the SPS at CERN with 400 GeV energy could be used. The corresponding neutrino energies will therefore still be limited to 350 GeV, although the flux will be unprecedented. A beam dump at the LHC could extend the energy range to the TeV scale, but the technology to operate such a facility is not presently available. Our proposal aims at measurement of neutrino properties in this previously unexplored domain above of 100 GeV.

The physics potential of a neutrino detector at LHC was discussed in a recent paper [18] where the TI18 tunnel was also identified as a suitable site to perform these measurements due to the very low machine-induced background. A fully passive detector based on the emulsion technology was also recently proposed there [19].

The importance of a configuration where the detector is positioned off the beam axis, slightly above the ideal prolongation of the LHC beam from the straight section, was recently underlined in [20]: in this configuration, the neutrino flux at high energies is found to be dominated by

neutrinos originating from charm decays.

The same experimental setup also allows to pursue another important scientific goal – searching for Feebly Interacting Particles (FIPs) with masses in the GeV range. FIP searches are currently undergoing an explosion of interest [21]. This interest is also stimulated by the lack of any discovery in various direct detection dark matter experiments, which have reached unprecedented levels of precision, as well as in collider searches which have collected large data samples with increasingly sophisticated analysis techniques. The majority of these efforts are targeting dark particle masses from about 10 GeV to 1 TeV, leaving the lower mass range much less explored. The scarce sensitivity at lower masses is related to the difficulty of detecting the corresponding very soft recoils, given the expected non-relativistic nature of galactic dark matter.

On theoretical side, these developments also stimulated significant activity. Many models have been proposed which expand the interesting FIPs mass range to lower values (GeV and below), while still giving rise to the expected relic DM abundance. One of the most prominent concepts is the existence of a "dark sector", which communicates with the SM particles through a feebly coupled mediator (see e.g. [17, 21]).

A pioneer in the search for light DM via direct detection, the CRESST-III low-mass DM experiment [22] recently published its first result for DM masses below 1 GeV. It is about ten orders of magnitude weaker than the XENON1T results for DM masses of 10 GeV or higher (see Fig. 1 left). The SuperCDMS SNOLAB experiment has the potential to improve these constraints by about four orders of magnitude in the future [23], but its potential impact on the DM parameter space strongly depends on the DM nature and other parameters, as demonstrated in Refs. [24, 25] (see Fig. 1 right).

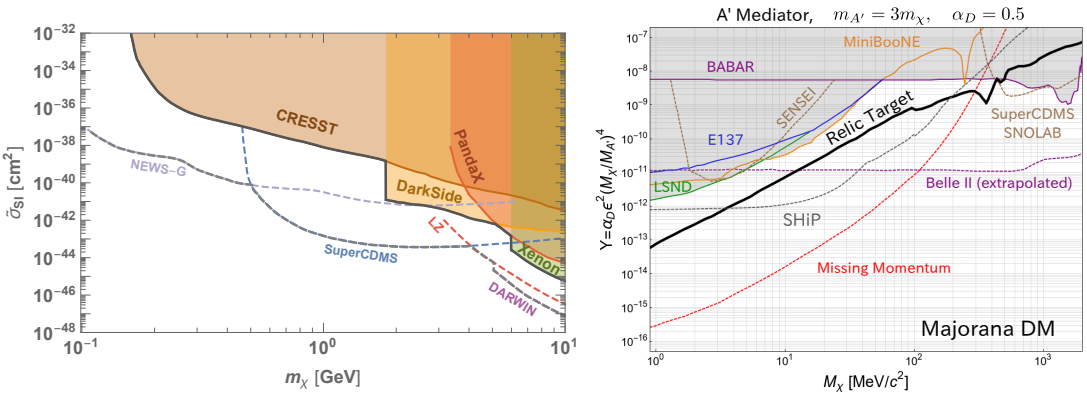

Figure 1: Left: Current (solid lines) and expected (dashed lines) constraints on the DM-nucleon scattering cross section from direct detection experiments [26]. Right: Direct detection experiments results (solid lines) and projections (dashed lines) translated to the same parameter space as accelerator-based searches for Majorana DM particles [24, 25]. Here the parameter y characterizes both the DM abundance in the early Universe, and the DM-nucleon scattering cross-section. On the x-axis m_χ is the DM mass. The DM particles χ are assumed to interact with the SM via vector mediator A'.

Despite these foreseen improvements, a large part of the FIP parameter space will remain unexplored. However, in the models with light mediators the limited sensitivity of direct

detection experiments can be mitigated by the searches of high-energy, beam-induced FIP particles.

LHC experiments, such as ATLAS, CMS or LHCb have limited sensitivities towards such searches. Indeed, the visible decay modes of a light DM mediator are either outside the detector due to the long lifetime, or suffer from very large backgrounds in the low-mass mediator region that is relevant from the relic abundance point of view. Invisible decays of light DM typically produce quite low missing-momentum, as the dominating production mechanisms do not give a significant boost to the DM particles. Additional handles such as associated hard jets or vector boson production lead to increased model dependence and significantly suppress the cross section that can be probed.

The most competitive results for light FIP searches therefore come from experiments based on electron beams that are able to control their backgrounds and precisely measure the energies of the final state particles in the events. These would include b-factories, such as BaBar and Belle in the past or Belle II [27] in the future, which employ the missing-mass technique; missing energy experiments at fixed target facilities, such as NA64 [28] operating at the CERN SPS; or the proposed LDMX experiment [24]; and, finally, FIP scattering experiments to be operated at high-intensity proton beams, such as the proposed SHiP facility [16, 17].

Here we propose an experiment to take data during Run 3 of the LHC. The detector is based on the Scattering and Neutrino Detector (SND) architecture proposed for SHiP [16, 29]. The detector will measure the neutrino energy and identify all three neutrino species in an unprecedented energy domain (between 350 GeV and few TeV). Given the pseudo-rapidity range accessible in this cavern, the detector will be off-beam-axis and the corresponding neutrinos will mostly come from charm decays, as shown in [20]: the proposed experiment will thus make the first test of the heavy flavour production in a high pseudo-rapidity range that is not accessible by the current LHC detectors. The identification of the three species and the measurement of the energy spectrum will enable muon and electron neutrino contributions to be disentangled, and a first ever estimate to be made for heavy quark production in the forward region. This measurement will allow the study of quantum chromodynamics effects in an unexplored domain, which has significant implications for the simulation of heavy quarks produced in atmospheric swarms that are initiated by cosmic rays [30]. In addition, given the timing performance of the apparatus, we will be able to search for FIPs coming from the LHC.

2 Complementarity with FASERν

The FASER collaboration [31] is planning to measure neutrino interaction cross-sections with a detector located in the TI12 twin tunnel, FASERν [32]. We outline here the complementarity of the physics case and compare briefly the detector technologies.

Unlike FASERν, the SND detector will be located off-axis. This location intercepts a different component of the neutrino flux, being more sensitive to neutrinos produced in heavy flavour decays, mostly charm; the importance of an off-beam-axis setup is discussed in a recent paper [20]. This thus gives insight into heavy quark production in a pseudo-rapidity range that is still unexplored, because it is far beyond the reach of current LHC experiments. The SND will in fact measure the $pp \to \nu X$ cross-section where neutrinos can be seen as a probe of the charm quark production, in the $7.2 < \eta < 8.7$ range. In particular, electron and tau neutrinos will uniquely come from heavy quark decays while muon neutrinos also come from pion and kaon

decays. The muon neutrinos from pion and kaon decays show a much softer energy spectrum: the energy measurement allows recognising the two components and comparing the result with electron neutrino data. In the on-axis location explored by FASERν, $\eta > 9$, neutrinos are mostly produced from pion and kaon decays. The combination of measurements performed in different η regions by the two experiments will allow for a better evaluation of systematic errors in the neutrino flux determination and in the evaluation of machine backgrounds. The use of the same simulation tools by the two experiments will be an essential ingredient for the comparison of the results on neutrino studies.

From the detector point of view, FASERν will be located in the space left available by the FASER apparatus. The detector will be essentially passive, being made of a 1.3 m long emulsion/tungsten target, followed at the very downstream end by a single station of silicon strip trackers, acting as interface layer between FASERν and FASER. The SND detector, instead, exploits all the available space in the TI18 tunnel and it was specifically designed for neutrino detection and dark matter search. Its layout and detector technology were optimised for the detection of three neutrino flavours. The target has a hybrid structure, being made of a sequence of 5.6 cm thick emulsion/tungsten walls interleaved with high-precision tracker stations made of 250 μm diameter Scintillating Fibres. Such a fine sampling of the target region (every $\sim 0.5\lambda_{int}$) provides high performance in the matching with electronic detectors, being independent of the hadronic shower development, and in the calorimetric measurement of electromagnetic and hadronic showers. As pointed out, the energy measurement is a key ingredient to interpret the data. The high sampling of the target region with high-precision timing detectors is the key feature to search for dark matter through its scattering with electrons and nuclei, otherwise impossible.

The muon detector located downstream of the target region allows the identification of the charged lepton in ν_μ CC interactions with high efficiency and purity since it offers on average 9.5 interaction lengths to the tracks originated in neutrino interactions. The superior performance in the muon identification and energy measurement reflects into a better identification of the different neutrino components, through the charged-current (flavour sensitive) process.

3 Overview of the experiment

In the pseudo-rapidity range that will be covered, $7.2 < \eta < 8.7$, electron and tau neutrinos originate practically only from heavy quarks, while the softer component of the muon neutrino flux is also produced by pion and kaon decays, as demonstrated in [19, 20]. The flux of muon, electron, and tau neutrinos versus their pseudo-rapidity and energy is shown in Fig. 2, as simulated with DPMJET3 (Dual Parton Model, including charm) [33] embedded in FLUKA [34, 35]. The heavy flavour production can be determined by measuring the yield of electron neutrinos. Assuming the SM cross-section for this species and the measured branching fractions for heavy flavour to ν_e, one can estimate the flux of the other neutrino species induced by heavy flavour production. This will allow the SM predictions to be tested and a search to be made for non-standard and flavour-specific neutrino interactions at high energies. In addition, the sensitivity to exotic scenarios, such as non-standard neutrino interactions and/or oscillations into light sterile states, will be studied.

The other goal of the project is to search for light FIPs through their scattering off the atoms. Thanks to the fast timing, searches for FIPs producing nuclear recoil or higher multiplicity events will be free of background in a large momentum and mass range. The sensitivity studies

are yet to be completed, but significant improvements can be expected, especially for models with Dark Scalar mediators interacting predominantly with nuclei.

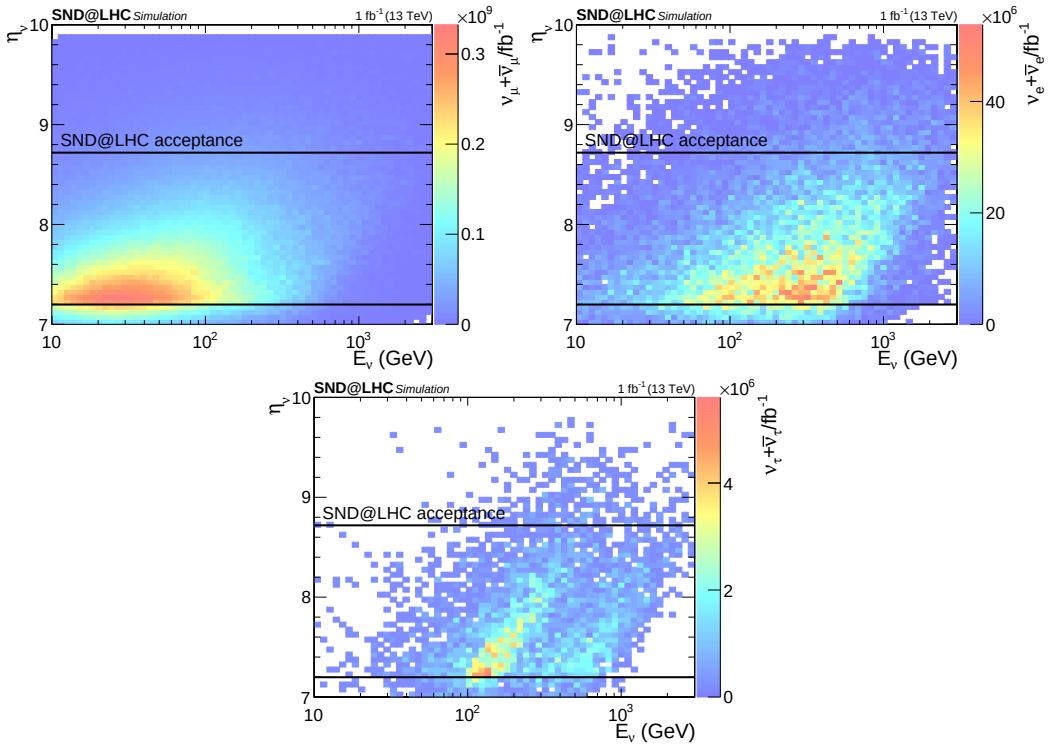

Figure 2: Neutrino flux as a function of ν energy and pseudorapidity for muon (left), electron (right) and tau (bottom) neutrinos.

The challenging task of identifying the three neutrino flavours and FIP scattering requires the construction of a hybrid detector, which combines nuclear emulsion technology and electronic detectors. A schematic view of the proposed detector is shown in Fig. 3. The detector consists of a target region followed by a muon identification system. The target region is instrumented with nuclear emulsions and Scintillating Fibre (SciFi) planes. Upstream of the target region a plane of scintillator bars will act as a veto for charged particles. The muon identification system is located downstream of the target. It will consist of iron slabs interleaved with planes of scintillating bars.

The emulsion detector, designed according to the Emulsion Cloud Chamber (ECC) technology, will act as a vertex detector with micrometric resolution, measuring all the outgoing charged tracks. The SciFi detector will predict the location of the neutrino interaction in the emulsion brick and will complement emulsion for the calorimetric measurement of electromagnetic showers. The SciFi will also connect the emulsion track with the muon candidate track identified by the muon detector, thus allowing for the identification of muon neutrino charge-current interactions. Moreover, the combination of SciFi and scintillating bars of the muon detector will also act as a non-homogenous hadronic calorimeter for the measurement of the energy of the hadronic jet produced in the neutrino interaction and hence for the neutrino energy.

The detector will be installed in the TI18 underground cavern, which has been identified as a suitable location in terms of machine-induced background [18].

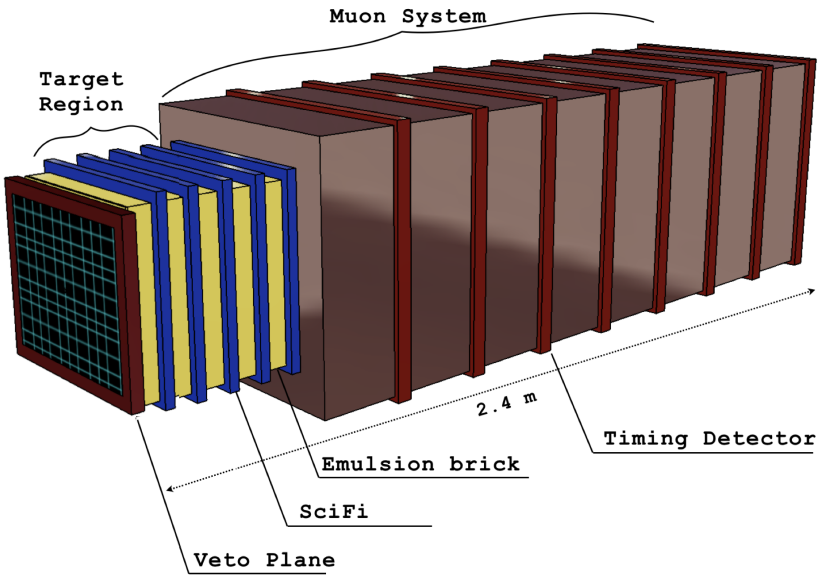

Figure 3: Schematic view of the Scattering and Neutrino detector.

In charged-current interactions, the identification of the neutrino flavour will be made by identifying the charged lepton produced at the primary vertex. Electrons will be clearly separated from π^0's thanks to the micrometric accuracy, which will enable photon conversions downstream of the neutrino interaction vertex to be identified. Muons will be identified by the electronic detectors as the most penetrating particles. Tau leptons will be identified topologically in the emulsion, through the observation of the tau decay vertex, together with the absence of any electron or muon at the primary vertex, according to the technology developed by OPERA [36, 14]. Figure 4 shows the display of an electron and a tau neutrino candidate reconstructed in the emulsion detector of the OPERA experiment.

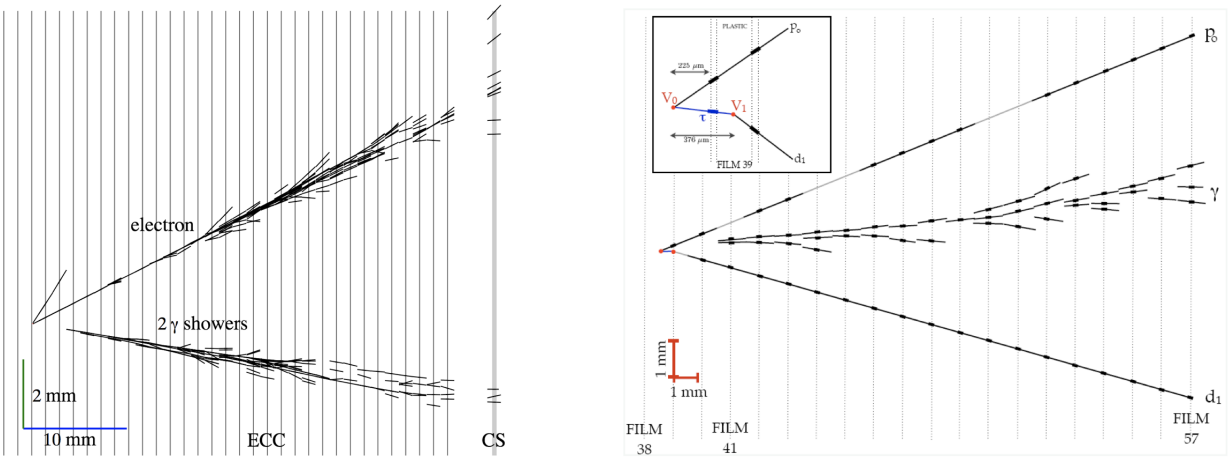

Figure 4: Display of reconstructed tracks in the OPERA emulsion detector for a ν_e (left) [37] and a ν_τ (right) [38] candidate event.

FIPs will be identified through their scattering off atoms of the emulsion target material. In the case of a FIP elastic scattering off atomic electrons, the experimental signature consists in an isolated recoil electron that can be identified through the development of an electromagnetic shower in the target region. The scattering off nuclei will be also exploited.

A detailed description of emulsion detector performances in neutrino and FIPs detection is reported in Section 7.

The data taking will start in 2022 along with the LHC Run3.

A target mass of about 810 kg will be installed, covering the pseudorapidity range $7.2 < \eta < 8.7$. The target will consist of five walls, each instrumented with a 40×40 cm^2 SHiP-like brick (with 1 mm thick tungsten plates) and followed by a 40×40 cm^2 SciFi plane. The muon detector will consist of eight iron walls, for a total of 8 interaction lengths, interleaved by the same number of planes made of scintillator bars. The planes of scintillator bars will have a timing resolution better than 100 ps for the time-of-flight measurements of particles from the ATLAS interaction point. The resolution in the time-of-flight measurement will thus be determined by the 200 ps due to the spatial distribution of the particle bunches. The granularity of the bars in the three most downstream planes will be increased in such a way to improve the efficiency of the isolation criteria for the identification of penetrating muons. To this aim, the three most downstream planes will also be equipped with an additional plane with bars oriented in the orthogonal direction.

We foresee the replacement of the emulsion target every 25 fb^{-1}. This replacement can be performed within the technical stops, since it requires a short access.

The muon system downstream will filter out hadrons; muons will be left as the only penetrating particles. The hits of the muon system and those of the SciFi tracking station will have to be combined for the energy measurement of the hadronic shower induced by a neutrino interaction.

Measurements already performed [18] foresee an expected charged particle rate in Run 3 lower than 0.1 Hz/cm^2. On the other side, the detector will have to be protected from the thermal neutron flux with a dedicated shield. Given the expected neutron fluence of 4×10^6/cm^2/fb^{-1} [18], a few centimetres of boron carbide will be sufficient. The use of silicon trackers in the target region for possible future upgrades might be tested during Run3.

4 Experiment conceptual design

Figure 5 shows the design of the detector. Both the side and top views are shown. Notice that the floor is inclined as it can be seen in the side view. For the target region, the electronics of the SciFi detector is also illustrated. Figure 6 shows the detector in the transverse plane.

4.1 Upstream veto

The Upstream Veto Detector, shown in Figure 7, will act as a veto for charged particles and will be located upstream of the Emulsion/SciFi detector.

The baseline technology for the Upstream Veto Detector is scintillating bars read out by silicon photomultipliers (SiPM). The detector will cover an active area of 42×39.9 cm^2. It will comprise seven vertically staggered EJ200 plastic scintillating bars, each with dimensions of $42 \times 6 \times 1$ cm^3 with a 3 mm overlap between bars. Light generated in the bars by traversing particles will be collected and read out by an array of eight SiPMs on both ends. Each array

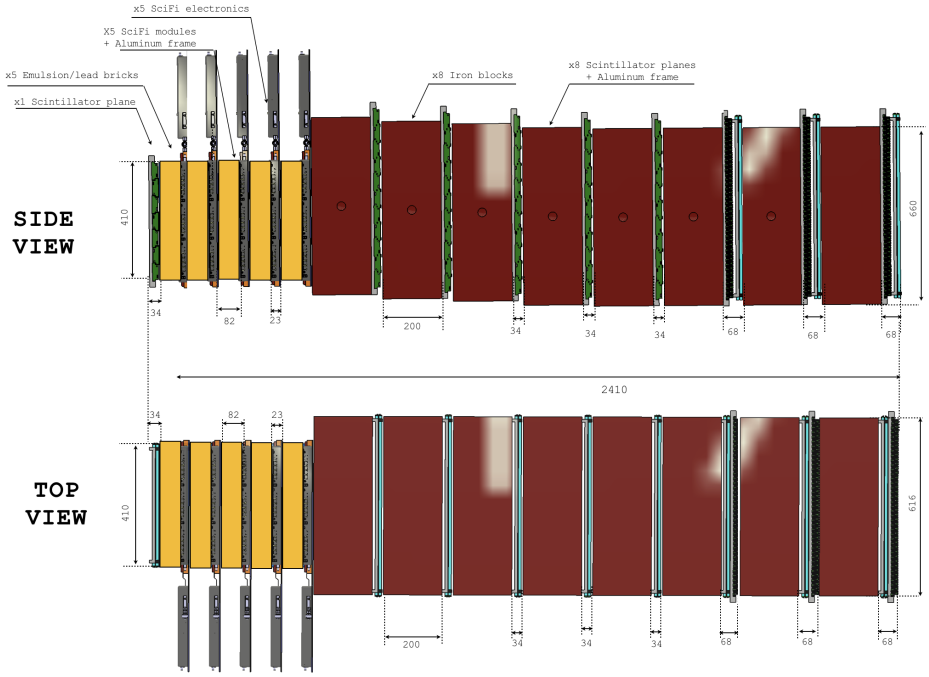

Figure 5: Overall setup of the SND.

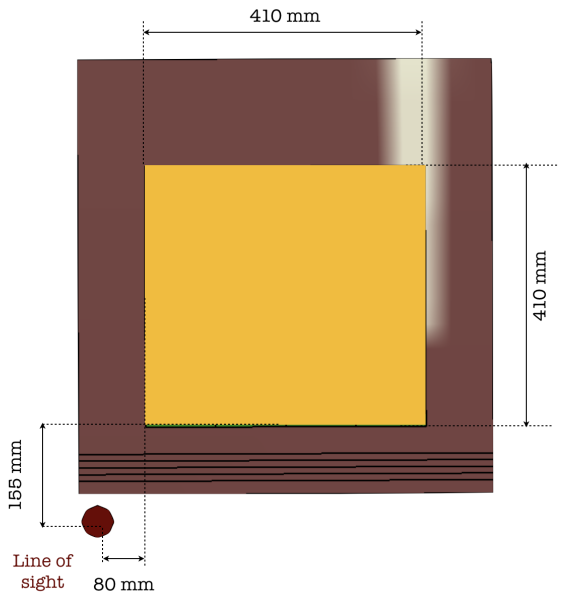

Figure 6: Frontal view of the detector.

of SiPMs will be read out by a custom made pre-amplifier PCB and the analogue signals will be subsequently digitised by a SAMPIC ASIC [39].

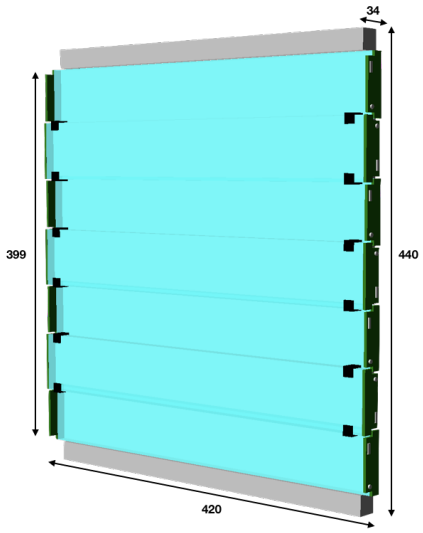

Figure 7: Illustration of the Upstream Veto Detector. Units of the labels are in mm.

The material for the scintillating plastic was chosen according to the timing resolution requirements. EJ200 is found to have the right combination of light output, attenuation length (3.8 m) and fast timing (rise time of 0.9 ns and decay time of 2.1 ns). The wavelength emission spectrum peaks at 425 nm, closely matching the SiPMs spectral response. The number of photons generated by a minimum-ionising particle crossing 1 cm of scintillating material is $\mathcal{O}(10^4)$. The bars will be wrapped in an aluminum foil and a black plastic stretch film on top to ensure opacity.

The aluminium support frame will consist of two vertical columns supported on top and bottom by horizontal bars. Plastic supports for the scintillating bars will be attached to the vertical columns. The entire support frame can be seen on the left side of Figure 8 and an example of how the scintillating bars will be fixed to the support is shown on the right side of Figure 8.

This technology has already been shown to act as a timing detector with resolution in the 10-100 ps range [40, 41]. The design is based on the SHiP timing detector, where bars of 168 $\times$ 6 $\times$ 1 cm^3 are read out on both ends by arrays of SiPMs. A 22 bar prototype of this detector was built and tested in summer 2018 and a timing resolution of 85 ps was achieved using the weighted mean from both ends of a single bar, as seen in Figure 9. Extrapolating these results to the length of the bars for the upstream veto detector gives an expected timing resolution of $\sim$ 50 ps. Our requirement of 100 ps is therefore conservative.

4.2 Emulsion target

The Emulsion target is made of five emulsion brick walls and five Target Tracker planes. Each wall has a transverse size of 410$\times$410 mm^2, consisting of Emulsion Cloud Chambers (ECCs) as illustrated in Figure 10.

The ECC technology makes use of nuclear emulsion films interleaved with passive absorber layers to build up a tracking device with sub-micrometric position and milliradian angular

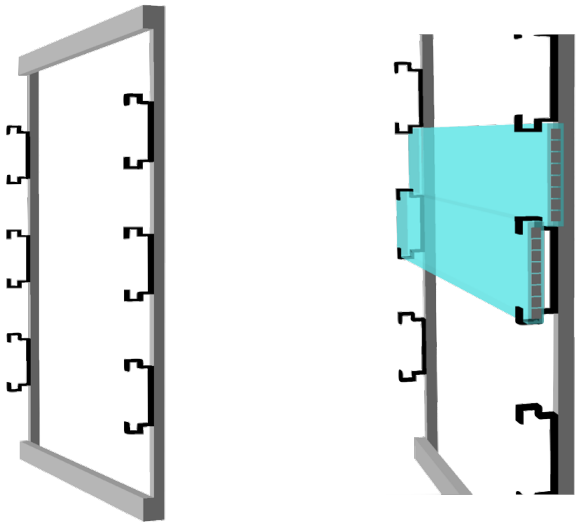

Figure 8: Left:Aluminium frame of the veto detector with plastic supports for the scintillating bars. Right: Illustration of how the scintillating bars will be supported on the aluminium frame. The location of the eight SiPMs on the end of the bars is also shown.

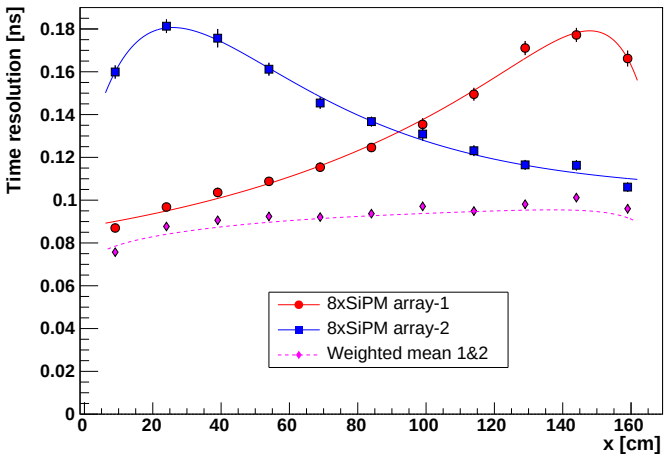

Figure 9: Time resolution as measured by the SiPM arrays at both ends of a 1.68 m bar as a function of the beam impact position along the bar [42].

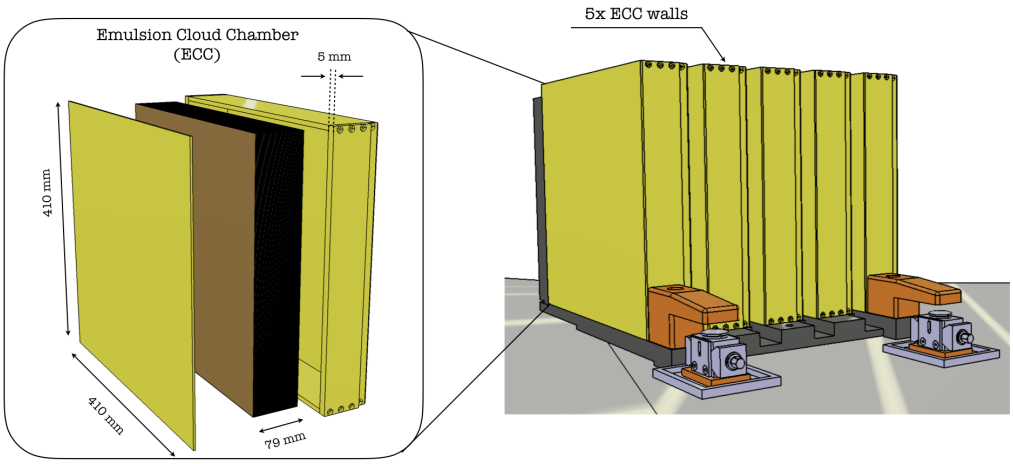

Figure 10: Layout of the emulsion target, consisting of five walls.

resolution, as demonstrated by the OPERA experiment [13]. It is capable of detecting τ leptons [14] and charmed hadrons [43] by disentangling their production and decay vertices. It is also suited for FIP detection through the direct observation of their scattering off electrons in the absorber planes. The high spatial resolution of nuclear emulsion films allows identifying electrons by observing electromagnetic showers in the brick [15]. Nuclear emulsion films are produced by Nagoya University and by the Slavich Company in Russia. For the long-term stability of the emulsion films, the temperature of the target will be kept at 15°C.

A unit cell is made of 57 emulsion films with a transverse size of 400×400 mm^2, interleaved with 1 mm thick Tungsten layers. The resulting brick has a total thickness of $\sim$8 cm, corresponding to $\sim18X_0$, and a total weight of $\sim$162 kg. The overall target weight with five walls is about 810 kg. Emulsion films are analysed by fully automated optical microscopes [44, 45]. The scanning speed, measured in terms of film surface per unit time, was significantly increased in recent years [46, 47, 48]. R&D is still ongoing [49] to further increase the scanning speed.

4.3 Target Tracker

The scintillating fibre (SciFi) tracker technology is particularly well suited for large surface tracking in a low radiation environment and it will play a key role to deliver the physics goals of the experiment. It allows to disentangle piled up events in the emulsion and it provides both time and energy information to the tracks and showers and associate these to the recorded events in the emulsion films. The SciFi detector technology for the target tracker, fibre mats and photo detectors, were developed by the EPFL group for the LHCb tracker upgrade [50]. While the SciFi provides tracking measurements for charged particles in the LHCb experiment, it serves several more purposes in the SND. Firstly, thanks to its spatial resolution of the order of 50 μm, it will connect tracks reconstructed by the electronic detectors with the corresponding tracks seen in the emulsion, thus providing the time stamp to the particle interaction detected in the emulsion films. It will also act as an active part of a sampling calorimeter of 90 radiation lengths, X_0, depth made together with the ECC bricks. Moreover, the target region and the downstream muon system form together a hadronic calorimeter, with about 11 interaction

lengths, λ. Therefore the SciFi plays an important role in the energy measurement of the hadronic and electromagnetic jets induced by the incident particle interaction.

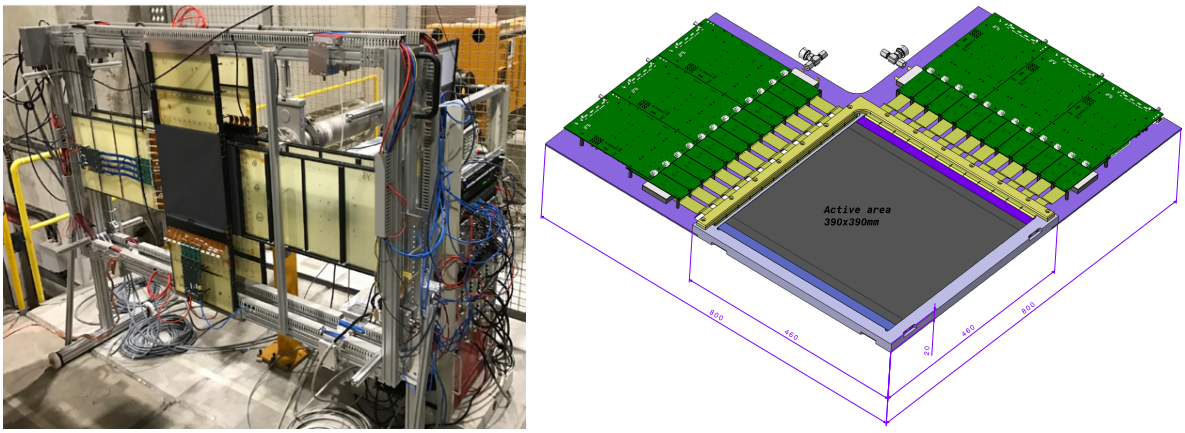

Figure 11: (left) SHiP-Charm SciFi modules equipped with readout. (right) A SciFi X-Y detection module with its corresponding readout electronics and the water cooling system for the front-end ASICs.

Four x-y SciFi planes equipped with the readout electronics, have been produced for the SHIP-Charm experiment [51], and may be used in the SND run in 2022 (Fig. 11 left).

The detection layers are based on the blue light emitting Kuraray SCSF-78MJ scintillating fibres of 250 μm diameter with a decay time of 2.8 ns. The layers are made of six densely packed staggered fibre layers glued together forming fibre mats of 133 mm width and 390 mm length; three fibre mats are integrated to a fibre plane with less than 500 μm dead zones between mats (Fig. 11 right). The readout channel segmentation with 250 μm wide channels is provided by a customised 128-channel SiPM array developed by the EPFL group with Hamamatsu for the LHCb experiment. A total of about 3000 channels is required for an X-Y module in the target tracker. The readout is situated outside the acceptance and consists of the photo-detector located at the fibre module's edge, a short Kapton flex PCB and the front-end electronics board. Light shielding of the assembly is ensured by a seal implemented at the flat Kapton flex section enclosing the photo-detectors and the entire fibre region. This part does not require any cooling as the heat dissipation of the SiPMs is sufficiently low. For time calibration and threshold adjustment, a light injection system is placed on the opposite side of the photo-detector fibre end. For the time measurement with the SciFi, a readout system based on the STiC ASIC [52] has been developed and tested in several testbeam campaigns during 2018-2019. A coincidence time resolution (CTR) of 350 ps between two planes of size 133 mm$\times$133 mm has been demonstrated with minimum ionizing particles. This corresponds to a single plane time resolution of about 250 ps. In case of the calorimetric operation of the SciFi, which leads to an order of magnitude more photons produced in fibres, further improvement of the time resolution is expected. An FPGA on the readout board collects the hit information of the STiC chips and it assembles them into larger frames. The FPGA handles the interface between the front-end and the DAQ CPU over a Gigabit Ethernet for data acquisition and slow control. The hit detection efficiency of the SciFi is expected to be larger than 99% for large planes, since no radiation damage will occur during the operation of the detector.

4.4 Muon and timing detector

The muon and timing detector is located downstream of the ECC/SciFi detector and it will identify muons, crucial to identifying muon neutrino charged-current interactions. In combination with the SciFi, it will serve as a non-homogeneous hadronic calorimeter, enabling measurement of the energy of hadronic jets. The timing resolution of about 100 ps per hit will allow to timestamp tracks in the SciFi and emulsion by linking them to tracks in the muon system.

Eight scintillating planes will be interleaved between layers of iron slabs 20 cm thick, which will act as passive material. The first five planes are similar to the upstream veto detector, albeit with different dimensions, and will be used as a timing detector for traversing particles. The last three planes consist of two layers of thin bars, one arranged horizontally and one arranged vertically, allowing for a spatial resolution less than cm. Muons will be identified as being the most penetrating particles as described in section 7.2. A schematic representation of the muon identification system is shown in Figure 12 while the layout of the upstream and downstream planes is reported in Figure 13.

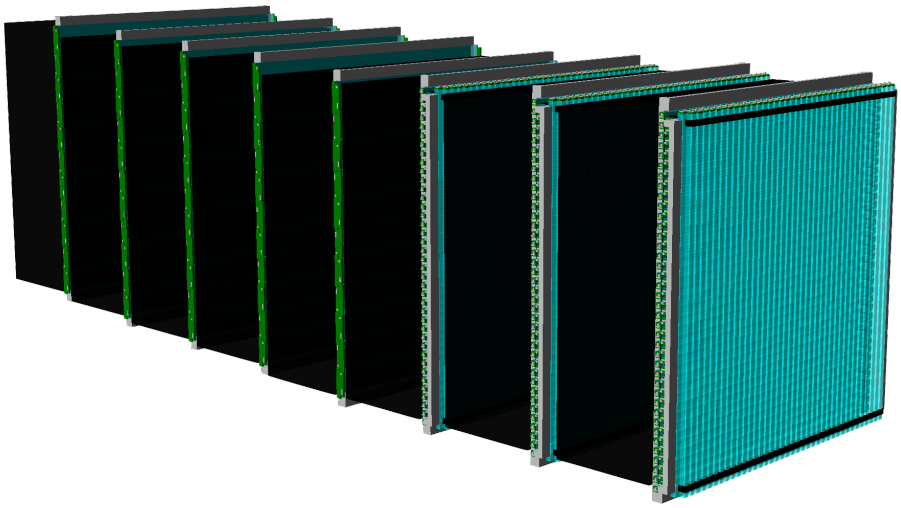

Figure 12: A schematic representation of the muon and timing detector.

The five timing layers comprise 11 bars, each with dimensions 62 × 6 × 1 cm^3 with a 5 mm overlap between bars. Each layer covers an active area of 62 × 60.5 cm^2. Every bar is wrapped in an aluminum foil and a black plastic stretch film and read out by a custom pre-amp PCB housing eight SiPMs on both ends, similar in fashion to the upstream veto detector. The timing resolution of each timing layer is expected to only be slightly worse than the upstream veto detector.

The last three layers will each consist of two scintillating planes; one with bars arranged horizontally and the other with vertically arranged bars. Bars in both directions measure 62 × 1 × 1 cm^3 with a 2 mm overlap between bars. The horizontal bars are read out on each end by a single SiPM, while the vertical bars are read out only from the top due to constraints of the cavern floor.

In order to increase the spatial accuracy and therefore gain in the muon isolation and identification performance, the SND Collaboration foresees upgrading the last three muon planes

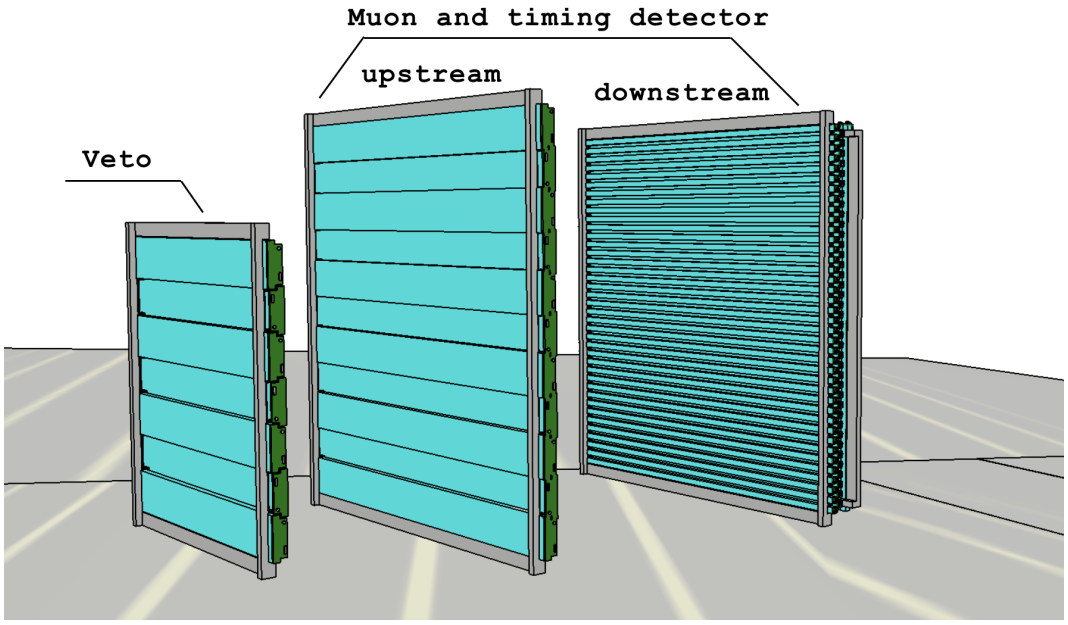

Figure 13: Layout of the upstream and downstream configuration of the muon and timing detector planes. The veto plane is also shown on the left side for comparison.

with tiles instead of bars, of the same type of those used by the CALICE Collaboration [53]. This upgrade will be performed during one of the long shutdown periods during Run3.

4.5 Data acquisition

The DAQ system close to the detector is composed of three parts, the fast control and timing signal distribution, two separate Gigabit Ethernet networks for the Timing detectors and the SciFi tracker readout and the slow control network for the infrastructure such as the cooling unit, temperature and radiation monitoring. The remote and strongly access restricted location as well as the power limitation at the TI18 cavern, suggests to locate the online data processing equipment on the surface. A possible location for a surface rack location where the online data processing and storage can be performed has been identified.

4.5.1 Acquisition mode

The signal from neutrino or dark matter particles is present only in a fraction of the target region and therefore only in one or several SciFi planes, making a hardware trigger implementation impossible. A data driven DAQ without trigger is imposed. All detector data, noise and physics event data, is transferred to the DAQ processor followed by a online data analysis for noise rejection and event building.

4.5.2 Timing and synchronisation

The synchronisation with the LHC machine will be implemented with the dedicated timing, trigger and control (TTC) systems. The TTC signal distributed on a single mode optical fibre has to be routed to the experimental site. The synchronisation signals Clock, Trigger and Reset will be made available for the synchronisation between the LHC, the timing detector and the

SciFi tracker. The time of flight of the detected particles can be extracted from the difference of the LHC clock and the particle hit time. The periodic injection of time calibration and synchronisation triggers will allow to verify the synchronisation of all electronics component over the long time run periods. For event building, all hit data is time stamped with a 32-bit long (LHC clock cycle unit, 25 ns) time counter representing a time interval of 107 s. The same time counter is sent to the DAQ up on a calibration trigger and allows for periodic verification of synchronisation.

4.5.3 Data rates and event processing

The data rates in the detectors are dominated by the noise data rate. For the timing detector the estimated data rate per 64-channel SAMPIC module is 150 Mbit/s and 2 Gbit/s for the system of 13 modules. For the SciFi tracker the expected hit noise rate per readout channel is 100 Hz (64-bit per hit). The number of channels for one SciFi X-Y plane is 3 K, with 4 planes the expected data rate is 80 Mbit/s. The data streams from the different modules are aggregated on a Gigabit Ethernet switch located in the detector rack and transmitted over 10 Gigabit Ethernet optical links to the DAQ server rack located on the surface. For the data transmission and control of the detector, two uplinks of 10 Gigabit are foreseen, providing sufficient margin for the future detector readout. Online data processing for noise suppression will be performed before data storage. The algorithm to perform the noise filtering can be based on the coincidence of hits in time and planes.

4.5.4 Equipment control and monitoring

A small amount of monitoring and remote controlled equipment will be located in the detector rack. A common cooling unit delivering water cooling for the SciFi and a air cooling for the Emulsion detector is remote controlled via Ethernet. All power supplies for the Timing detector and SciFi providing bias voltage for SiPMs and low voltage for the front end electronics is controlled and monitored via Ethernet as well as all additional temperature or radiation monitoring systems. It is not foreseen to have any local CPU located in the rack.

5 Detector integration in the TI18 cavern

Particular effort has been paid on the studies for the integration of the needed services, to guarantee a cost efficient design of the SND and to evaluate the feasibility of its installation inside the TI18 cavern. A preliminary study of the infrastructure requirements was performed and it was followed by a first iteration with the concerned CERN groups, in order to define the best installation strategy and the project requirements. A first proposal has been presented at the Intégration Cellule LHC meeting, which is in charge of the integration studies of the LHC machine, on February 12th 2020: no showstoppers and integration issues were identified.

The latest version of the detector with the corresponding installation plan was presented at a recent ICL meeting held on August 5th 2020 and the main recommendation was to install part of the services before the machine cool down. This is reflected in the preliminary installation schedule reported in Fig. 29.

Preliminary survey, electrical engineering, cooling and ventilation, transport, safety and radiation protection specifications were used to achieve the first integration of the SND as

shown in Figure 14.

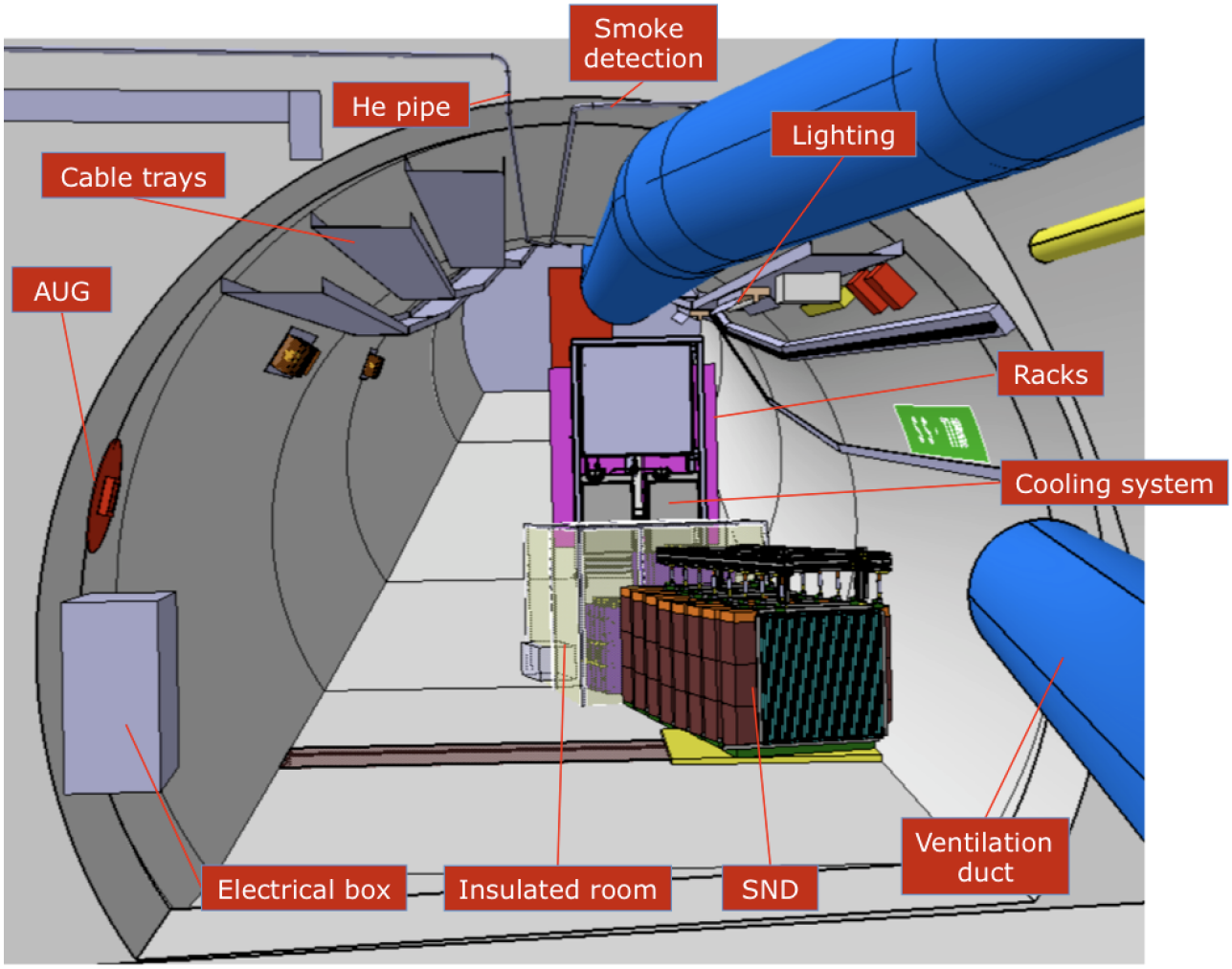

Figure 14: SND integration inside TI18

As described in Section 4.2, the temperature of the emulsion target must be below 15 °C in order to avoid possible fading effects. In addition, the SciFi needs **water-cooling** for its electronics. Therefore, the proposal includes two chillers located next to the detector and an insulated box equipped with an air fan. The chillers will provide cooled water to the electronics and to the air fan. The later will cool down the refrigerated volume taking the air from the tunnel. Figure 15 shows the conceptual scheme of the cooling system. A mineral wool layer or a fire barrier duct wrap can be used as insulator and aluminium profiles to build the structure of the insulated box. The structure should include a 3 cm-thick layer of boron carbide to keep the detector protected from thermal neutrons. The expected water-cooling power consumption is 2.5 kW.

It has been identified that a **ventilation** duct located inside the TI18 cavern has to be removed to avoid interference with the detector. A visit with EN-CV, RP, transport and the coordination teams was organised on December 2019 where it was concluded that the duct can be easily removed, with slight modifications on the existing infrastructure, and transported to the surface (see Figure 16). Samples will be taken and analysed by HSE-RP to check the activation of the ventilation duct prior its removal. Nevertheless, from the experience of

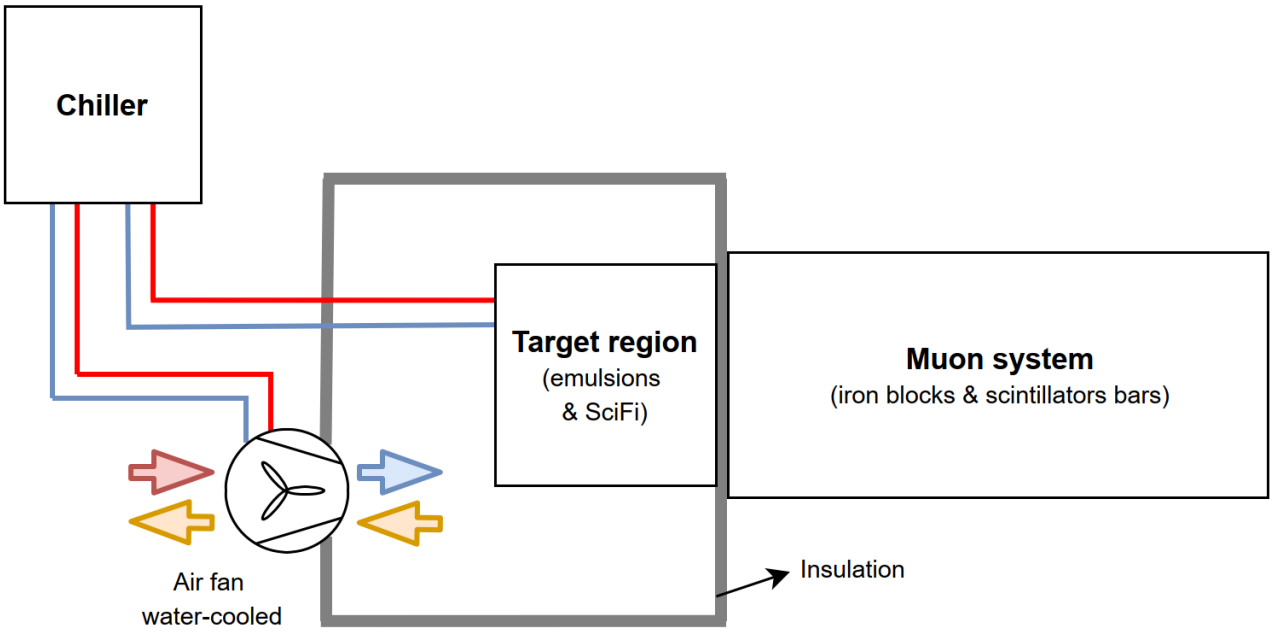

Figure 15: Proposed cooling scheme for the SND.

similar works conducted in TI12, the activation of such components is expected to be below the clearance limits (LL).

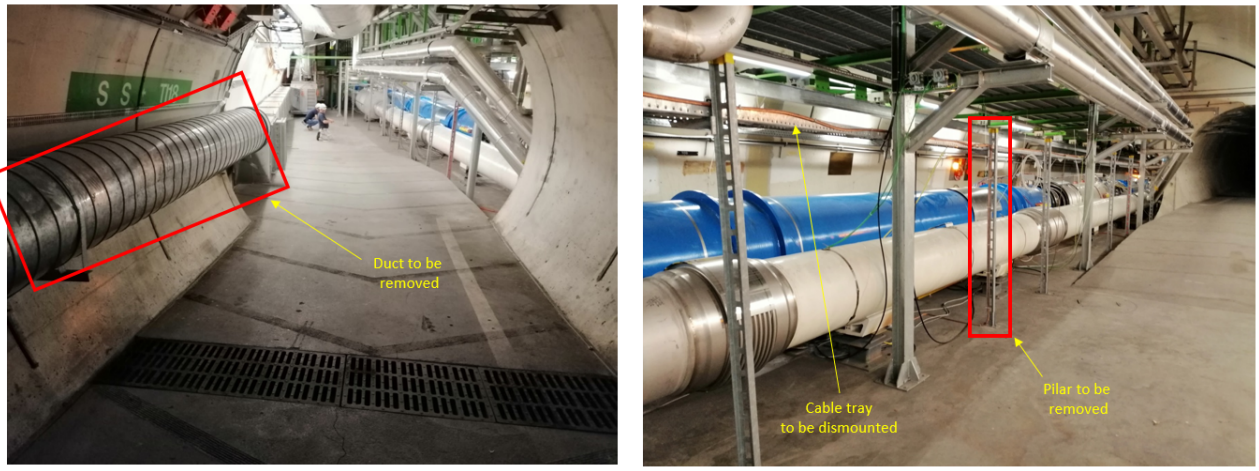

Figure 16: Activities to be carried out for the ventilation duct removal

The sub-components and services required to run the detector can be transported by a trolley from the surface level to the LHC tunnel through the PM15 elevator and, then, transported along the LSS1R to UJ18. Inside UJ18 the small parts can be passed below the LHC machine with a low trolley, where there is a free passage about 80 cm wide and 34 cm high, and finally, installed in TI18. However, there are a few components which have to be passed above the LHC owing to their dimensions. Therefore, a hoist with about 250 kg capacity is required. A protection structure (similar to FASER-UJ12 protection [54]) has to be installed for the protection of the LHC machine and cryogenic line. For the final installation of the heaviest parts, a specific handling equipment is required to climb the slope of the TI18 cavern. After discussion

and a site visit with the **transport** experts, no showstoppers have been identified. Table 1 includes the weight and dimensions of the most restrictive parts to be handled.

Table 1: The most restrictive sub-components to be transported

Part	Dimensions (cm)	Unit weight (kg)	Number of units
Veto plane	100 x 100 x 25	20	1
Muon detector			
SAMPIC boards	50 x 50 x 30	10	6
SAMPIC Power Supply	50 x 30 x 30	8	1
HV+LV supplies, crate	50 x 50 x 30	20	1
Veto plane	60 x 60 x 20	4	1
Muon timing plane	80 x 80 x 20	6	5
Muon x,y plane	80 x 80 x 20	8	6
SciFi			
Modules	100 x 100 x 25	15	5
Power supplies, crates, switch	50 x 50 x 30	20	6
Iron block	80 x 20 x 20	230*	32
Rack	50 x 50 x 170	25	2
Chiller	100 x 60 x 40	80	2
Emulsion brick	41 x 41 x 8.5	162	5

*It can be divided in smaller pieces to reduce weight and can pass below the LHC machine

The conventional **safety** aspects have been discussed with HSE-OHS group and no showstoppers have been identified. A PESS-correspondent has been assigned to follow the project and evaluate, together with the HSE-OHS specialists, the safety aspects in detail within the Coordination of Project Experiment Safety Support activities. Regarding the personnel space route, there is a bridge already installed above the magnet MBB13.R1 to pass over the LHC machine in case of an emergency. The Launch Safety Discussion document is under preparation in order to proceed with the release of the safety project requirements report.

A detailed **radiation protection** study has been launched by the HSE-RP to evaluate the radiation levels during TS and the activation of the SND components within the TI18 cavern, considering run 3 conditions. HSE-RP will provide a detailed radiological evaluation of the SND operation and maintenance in the coming months. The access of personnel over 1 or 2 days during the technical stop to replace the emulsion bricks seems feasible due to the relatively low activation risk expected in TI18 during Run 3. The exposure time of the bricks to cosmic rays has to be minimised, therefore, an effective plan among the transport, RP and detector teams has to be developed.

Radiation levels in TI18 are dominated by beam-gas interaction from the incoming beam, with the luminosity-driven losses in cells 11 and 13 of the dispersion suppressor for the outgoing beam being negligible. The measured radiation values during 2018 [55], scaled to a nominal Run 3 operation year, yield expected annual levels of 2e7 and 1e8 $cm^{-2}yr^{-1}$ HEHs and thermal neutrons, respectively. Such levels are almost an order of magnitude larger than the limits which EN-STI-BMI considers to declare an area as radiation safe for pure commercial electronics systems. However, it is to be noted that the limits consider distributed systems, whereas for a single unit system, they can be regarded as clearly pessimistic; and that the measured levels correspond to the intersection between TI18 and the LHC tunnel (UJ18) and equipment would

clearly benefit from being positioned some meters inside TI18. Therefore, the prospects are that commercial electronics in TI18 are expected to operate in radiation safe conditions, however, a more detailed study of the environment (i.e. 2D FLUKA maps with R2E quantities) and electronics type description would need to be carried out further ahead in the project for a final confirmation.

There is a clear line of sight to link the detector position with the LHC machine coordinate system. In order to do so, three **survey** fiducials per element to be measured or aligned are to be included in the detector set-up. They have to be as far away as possible from each other to ensure good quality measurements and they must be visible from a single fixed position. Every component that has to be aligned should be supported isostatically on 3 points. The first approach indicates that an absolute alignment and measurement accuracy of 1 mm is sufficient for SND purposes. The alignment and measurement accuracy among sub-components (i.e. SciFi plane, emulsion plane etc.) has been set to 0.2 mm.

A first conceptual design (see Figure 17) of the alignment strategy divides the detector in two independent assemblies:

- The target region is supported by a single support structure and aligned by three feet (the SPS magnet feet design [56] has been taken as reference). A kinematic system mechanically fixed by three points (a slot, a cone and a flat) to the support structure has to be designed for the emulsion and SciFi planes. Each wall will have a surface on the corner to place the survey fiducials. An emulsion wall is made of 12 bricks to be aligned mechanically by their own assembly frame. They can be fiducialized by a Romer arm on the surface if clear references (fiducial and/or surfaces) are included on the bricks.

- The muon system is supported by the iron blocks. A plate with three screws will be attached to the floor and aligned. By filling the space between the plate and the floor with concrete, the plate will be rigidly fixed to the floor. This operation will be done for the assembly of each iron block. After that, the iron blocks are piled up and positioned by space holders to keep the required space for the insertion of scintillators bar planes. On top of the assemblies and supported by three points fixed to two different iron blocks, there is a floating structure which will support the scintillator bar planes. Each scintillator bar plane is supported by three points (two on top and one on the side) and will need an available surface for the installation of fiducials.

The alignment system of the detector is being discussed with the alignment experts to find the best design complying with the specifications and guarantee a robust supporting system. The local gravity direction has been provided by the survey group for design purposes.

The preliminary requirements and **electrical services** have been identified in order to comply with the detector specifications. The total electrical power of 10 kW will be enough to supply the chillers, lighting equipment, SciFi, timing detector and racks. The electrical services addressed include: an electrical distribution box located at the entrance of the TI18 cavern, two AUG required for safety aspects, permanent lighting (about 3 normal lamps plus two anti-panic lighting) and x5 sockets of 220 V.

In relation to the signals, readout and networking infrastructure, the following items have been identified:

- Two 19' racks for the fibre optics connection modules, NIM crates and power supply for the detector components.

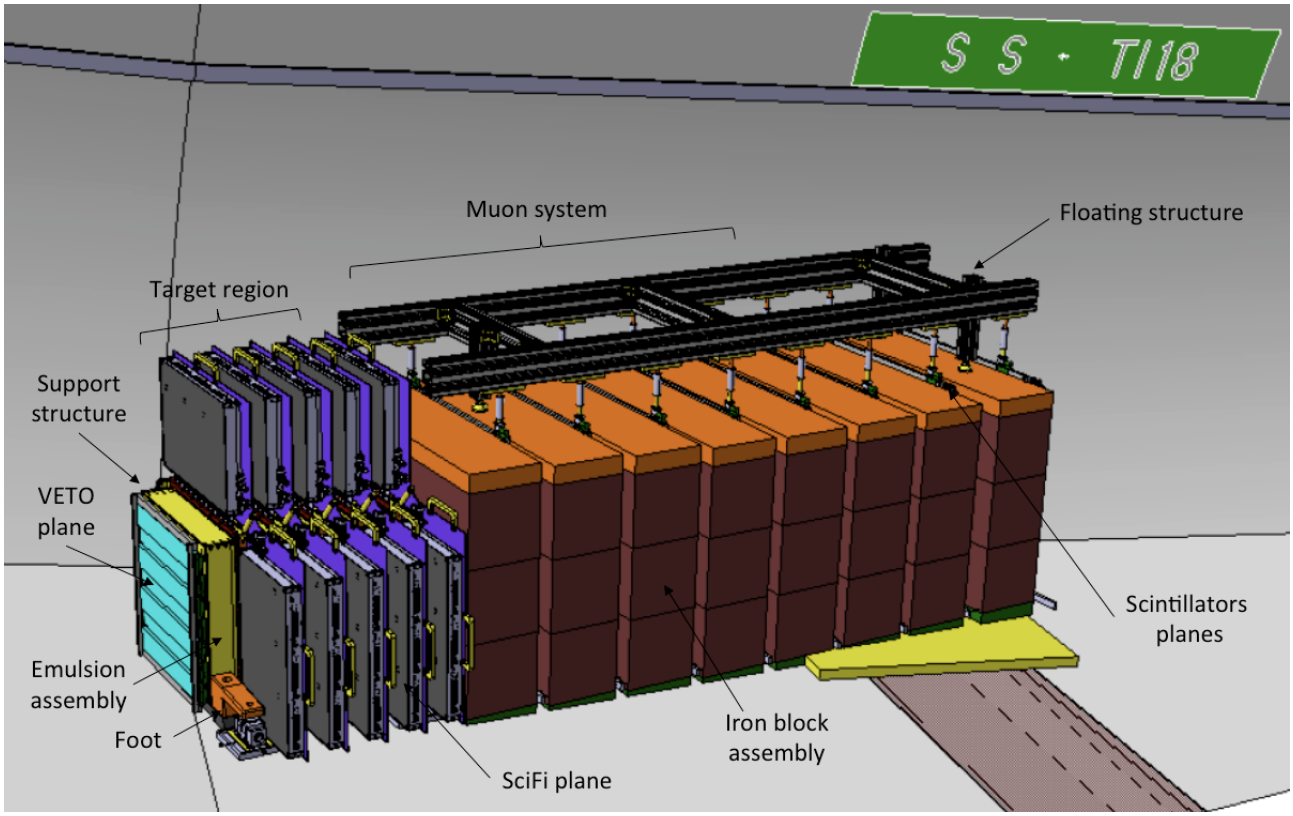

Figure 17: Detector layout pointing out the main concepts of the alignment system

- A rack on surface to host the server for data acquisition.
- A set of 12 fibre optics for the detector, Ethernet and cooling control system communication. The preliminary optical fibres layout is shown in Figure 18. It was considered preferable to avoid passing them along the Long Straight Section to avoid their de-installation and re-installation due to the HL-LHC upgrade during LS.

Very productive and effective discussions with EN-SMM, HSE-OHS, HSE-RP, EN-HE, EN-EL-EIC, EN-EL-FC, IT-CS-DO, EN-CV, IT/CS/CS, EN-STI-BMI, EN-ACE-INT, EN-EL-EWS concluded that the preliminary SND integration and installation of the required infrastructure are feasible.

6 Emulsion data analysis

6.1 Emulsion scanning and analysis

Emulsion films consist of two 70μm-thick layers of nuclear emulsion, separated by a 175 μm-thick plastic base. The transverse size is 40×40 cm^2, like for the passive plates.
The track left by a charged particle on an emulsion layer is recorded by a series of sensitised AgBr crystals, growing up to 0.6 μm diameter during the development process. A new generation automated optical microscope analyses the whole thickness of the emulsion, acquiring various topographic images at equally spaced depths. The acquired images are digitized, then an

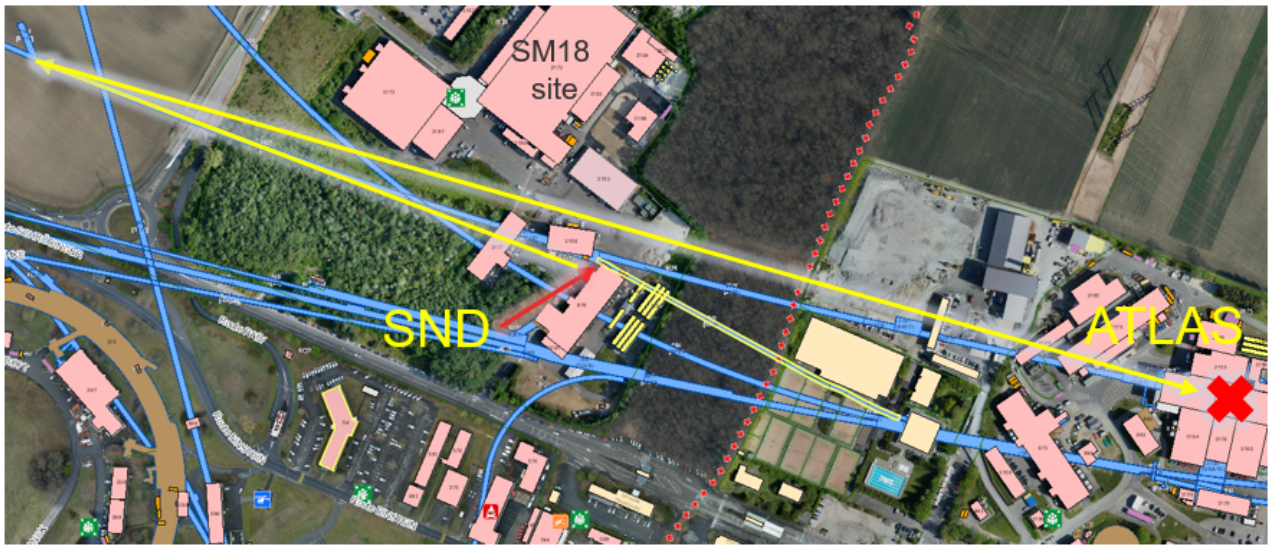

Figure 18: Preliminary optical fibres layout

image processor recognizes the grains as *clusters*, i.e. groups of pixels of given size and shape. Thus, the track in the emulsion layer (usually referred to as *microtrack*) is obtained connecting clusters belonging to different levels. Since an emulsion film is formed by two emulsion layers, the connection of the two microtracks through the plastic base provides a reconstruction of the particle's trajectory in the emulsion film, called *base-track*. The full-volume wide reconstruction of particle tracks requires connecting base-tracks in consecutive films. In order to define a global reference system, a set of affine transformations has to be computed to account for the different reference frames used for data taken in different films.
The analysis of emulsion films is performed using new generation optical microscopes. For the OPERA experiment two different scanning systems were developed: one in Japan, the Super Ultra Track Selector (S-UTS) [57], and one by a collaboration of the different European laboratories, the European Scanning System (ESS) [45, 44, 58, 59]. The ESS is a microscope equipped with a computer-controlled monitored stage, movable along both X and Y axes and in the Z direction, a dedicate optical system and a CMOS Mega-pixel camera mounted on top of the optical tube. For each field of view, it executes the following steps: local tomography, cluster recognition, grain selection, three-dimensional reconstruction of aligned cluster grains, parameter extraction for each grain sequence. The ESS allows the scanning of the whole emulsion surface with a maximum speed of 20 cm^2/h.
An upgrade of the ESS system was performed by the Naples emulsion scanning group [47]. The use of a faster camera with smaller sensor pixels and a higher number of pixels combined with a lower magnification objective lens, together with a new software LASSO [47, 46] has allowed to increase the scanning speed to 180 cm^2/h [48], more than a factor ten larger than before. The lens of the microscope guarantees a submicron resolution and, having a working distance in Z longer than 300 μm, allows for a scan of both sides of the emulsion film. In order to make the optical path homogeneous in the film, an immersion lens in an oil with the same refraction index of the emulsion is used. A single field of view is 800×600 μm^2; larger areas are scanned by repeating the data acquisition on a grid of adjacent fields of view. The images grabbed by the digital camera are sent to a vision processing board in the control workstation to suppress

noise.

6.2 The SHiP-charm measurement

The analysis tools recently developed by the SHiP collaboration for the SHiP-charm project can be applied for the analysis of emulsion data in SND. Although signal and backgrounds expected at SND are different from those from the SHiP- charm measurement, the two projects share the same challenging task of identifying interactions in an unprecedented flux of charged particles.

The SHiP Collaboration proposed the SHiP-charm project [51], aiming at measuring the associated charm production induced by 400 GeV/c SPS protons. This proposal includes a study of the cascade effect [60] to be carried out using the ECC technique. The detector is a hybrid system, combining the emulsion technique with electronically read out detectors and a spectrometer magnet to provide the charge and momentum measurement of charmed hadron decay daughters and the muon identification.

An optimisation run was performed at the H4 beam-line of the CERN SPS in July 2018 with an integrated number of protons on target of about 1.5×10^6. Lead was used as passive material for the ECC. Six different target configurations were used in order to measure the charm production along a depth corresponding to $\sim$2 interaction lengths: in this depth about 80% (50%) of the charm production from primary (secondary) interactions is expected.

Each ECC was mounted on a moving table in order to change the position of the target with respect to the proton beam and irradiate the whole surface of the detector. Figure 19 reports the characterisation of the proton beam in one of the ECC targets both in terms of angle (left) and position (right). The pattern observed in the position distribution reproduces the movement of the target with respect to the proton beam.

The number of protons impinging on ECC target units vary from $10^2/\text{cm}^2$ to $10^3/\text{cm}^2$ according to the configuration of the exposure. The data analysis shows that the track density increases with the depth in the module due to the proton interactions, hadronic re-interactions and electromagnetic showers, as shown in Fig. 20. The density of segments reconstructed in a single emulsion film extends up to $5{\times}10^4/\text{cm}^2$. The challenge of the SHiP-charm measurement is two-fold: reconstruct tracks and interaction vertices in a high density environment, and search for rare decays of charmed hadrons. The first challenge is also shared by the SND measurement where we expect to get an integrated density of track segments up to $10^5/\text{cm}^2$ for an exposure of about 25 fb^{-1}.

About 10^4 proton interaction vertices are expected in a single ECC target unit ($\sim 10^3/\text{cm}^3$). 400 GeV/c proton interactions produce on average 15 charged particles and 10 photons, having energies ranging from a few to tens of GeV. This results in a large number of secondary hadronic re-interactions and electromagnetic showers, that increases the number of reconstructed vertices up to $5{\times}10^5$. To set the scale, the unitary target of the OPERA experiment contained in the same volume a single neutrino interaction vertex.

The analysis of the SHiP-charm emulsion data therefore required the development of dedicated software and analysis tools to extract the signal from an unprecedented background rate. The results obtained for the reconstruction of proton interaction vertices in one of the ECC target units are reported in Fig. 21. A good agreement between data and Monte Carlo expectations is found, both in normalisation and in shape, for the number of charged tracks defining the interaction vertex and the position of the vertex along the beam axis. These results prove

the capability to reconstruct interaction vertices in a harsh environment.

The search for charmed hadrons is based on the observation of a decay topology in a ∼55 mm^3 volume downstream of each interaction vertex and relies on the measurement of topological and kinematic variables at the secondary vertex. The required background suppression is of the order of 10^4 and specific analyses are being developed to enhance the signal-to-noise ratio. Figure 22 shows an example of a double-charm candidate event that has three vertices: the most upstream is the proton interaction vertex. There are two additional vertices: one shows a two-prong topology without any charged parent particle while the other one shows a kink topology.

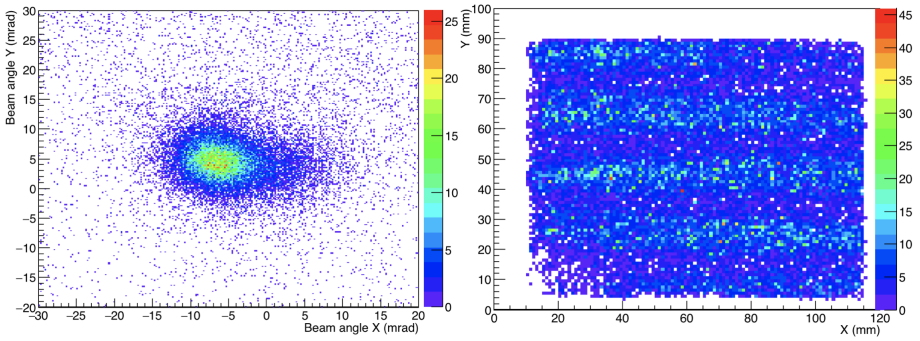

Figure 19: Left: angular dispersion of the proton beam as reconstructed in one of the exposed ECC target units. Right: position distribution of the incoming protons on the emulsion surface.

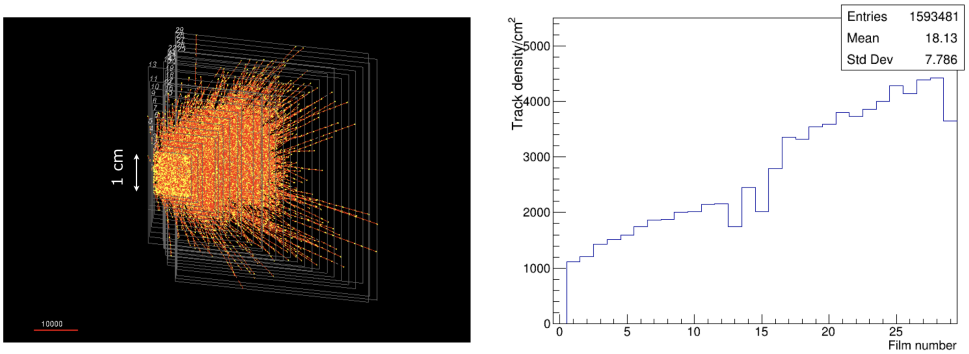

Figure 20: Left: Tracks reconstructed in a 1×1 cm^2. Right: track density in one of the exposed ECC target units.

7 Physics performance

7.1 Simulation Software

The simulation of the SND is handled by the FairShip software suite, developed within the SHiP collaboration, which is based on the FairRoot software framework [61].

Neutrinos production in proton-proton collisions at the LHC is simulated with DPMJET3 (Dual Parton Model, including charm) [33] embedded in FLUKA [34, 35], and particle propagation towards the detector is done through the FLUKA model of the LHC accelerator [62]

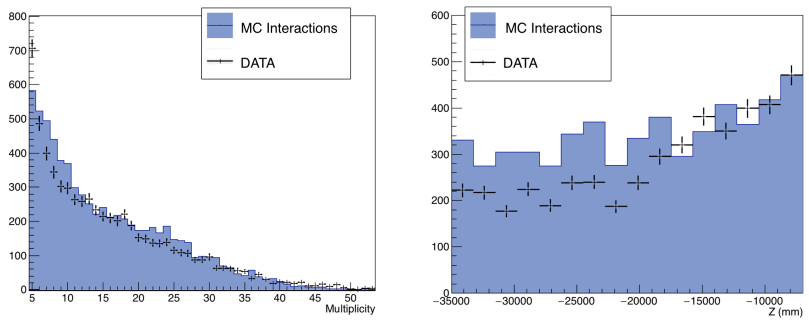

Figure 21: Charged track multiplicity and position along the beam direction for interaction vertices reconstructed in one of the ECC target units. Data points are in good agreement with Monte Carlo expectations.

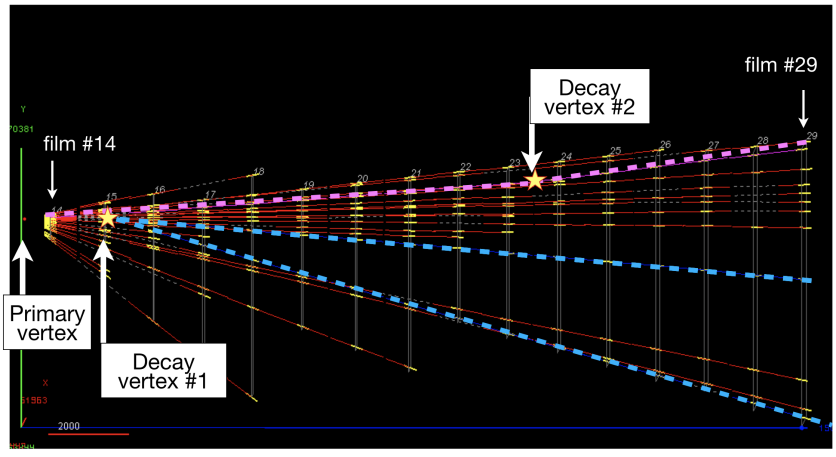

Figure 22: One of the double-charm candidates reconstructed in the ECC.

in order to simulate also neutrinos from further decay of collision and re-interaction products. GENIE [63] is then used to simulate neutrino interactions with the detector material. The output of GENIE is given to GEANT4 [64] for the particle propagation in the detector.

7.2 Neutrino physics

The neutrino detector covers a pseudo-rapidity range between $7.2 < \eta < 8.7$. The spectra and the neutrino yield at the neutrino detector for the three different neutrino flavours are reported in Fig. 23a and in Table 2. The muon rate is expected to be 100 Hz over the whole detector surface.

Assuming a luminosity of 150 fb^{-1}, the integrated neutrino flux for the different neutrino flavours at the target region is reported in the left column of Table 2 and the corresponding energy spectra are shown in Fig. 23a. The expected number of charged-current neutrino interactions occurring in the detector is reported in Table 2, while the energy spectra are shown in Fig. 23b. Expectations are compatible with those evaluated in the pseudo-rapidity range between $7.4 < \eta < 9.2$ and reported in [20].

Table 2: (Third column) Integrated neutrino flux for 150 fb^{-1} for the different neutrino flavours at the target region. (Fifth column) Expected number of CC interactions for the different neutrino flavours for 150 fb^{-1}.

Neutrino flavour	⟨E⟩ GeV (incident)	Neutrino Flux	⟨E⟩ GeV (interacting)	CC Interactions Updated config
ν_μ	140	2.6×10^{12}	430	783
ν_e	370	3.4×10^{11}	670	256
ν_τ	410	1.7×10^{10}	710	13
$\bar{\nu}_\mu$	150	2.3×10^{12}	480	324
$\bar{\nu}_e$	380	3.6×10^{11}	725	130
$\bar{\nu}_\tau$	390	1.7×10^{10}	740	5
TOT		5.6×10^{12}		1511

7.2.1 Neutrino detection

For the data analysis a fiducial volume inside the brick is selected, excluding the regions within 5 mm from the downstream edge and 1 mm from the lateral side. This results in a geometrical efficiency ϵ_{geom} of approximately 89.3%. The location of a neutrino interaction requires the presence of least one track with a momentum larger than 1 GeV/c attached to the primary vertex identified by two visible tracks in emulsion. The visibility criteria are listed in Tab. 3. Monte Carlo simulation studies, fully validated with data from the SHiP-charm measurement, have shown that the location efficiency for the different neutrino flavours is above 90%.

Muon Identification Muon identification is relevant for both identifying ν_μ and ν_τ interactions. As a matter of fact, charmed hadrons produced in ν_μ CC interactions constitute a

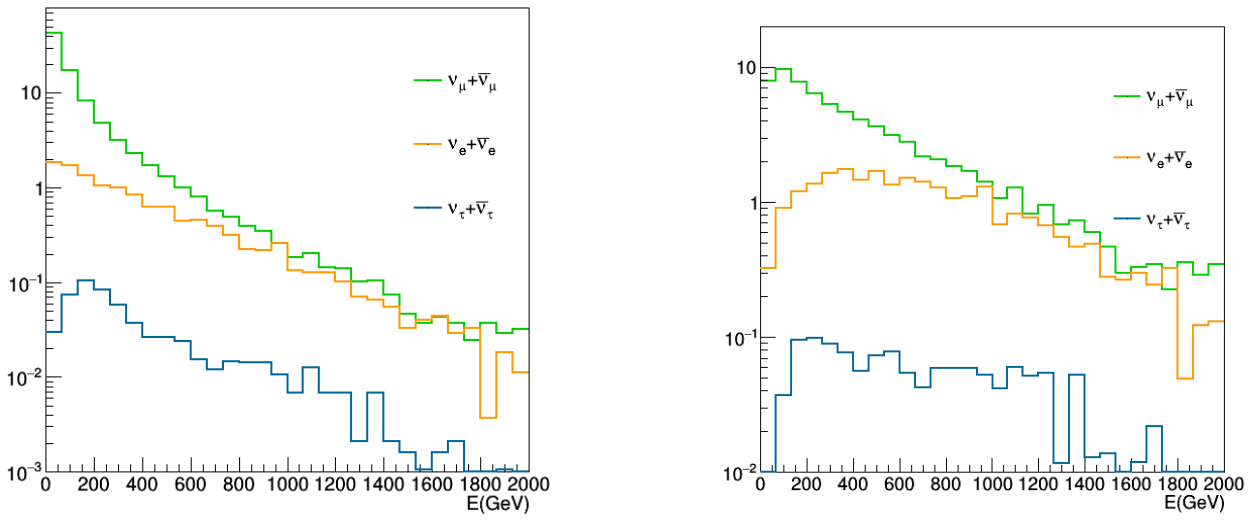

(a) (b)

Figure 23: Energy spectra of the three neutrino flavours at the target region (a) and interacting in the target region (b). The total number of neutrinos is normalised to 100.

Particle	Visibility cut p (MeV/c)
charged	> 100
p	> 170
π^0	> 400
γ	> 200

Table 3: Visibility cuts on the momentum of primary tracks at the neutrino vertex.

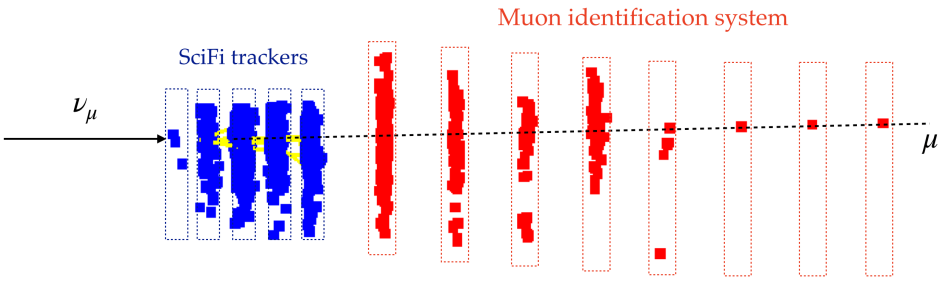

Figure 24: Simulated muon neutrino interaction. The muon exhibits isolated hits in the three most downstream planes of the muon identification system.

background for the ν_τ search if the primary muon is not identified. A display of a simulated ν_μ CC interaction can be found in Fig. 24.

MonteCarlo studies have shown that $\approx 98.4\%$ of the muons produced in ν_μ CC interactions enter the muon system. Out of them, $\approx 91.5\%$ leave a hit in the last three planes of the muon identification system and can thus be identified. The current algorithm is based on the tracks reconstructed in the emulsions at the neutrino interaction. Each emulsion track is projected on the last three muon detector planes, comprising both horizontal and vertical bars providing X-Y coordinates. The corresponding X-Y bars hit by the projected track on each of the three planes are identified. The primary track is considered found on a given plane if there is a corresponding hit in the bars corresponding to the projected track location or in the adjacent bars. Isolation of the track is determined by requiring no hits in the bars adjacent to the search window.

A muon candidate is selected according to the following criteria:

- A corresponding track is found on all the three most downstream muon detector planes.
- The track is isolated at least in two of the three planes.

The above selection results in a muon identification efficiency of about 77% for charged current ν_μ interactions. Accounting also for the geometrical acceptance described above, the overall muon identification efficiency is $\sim 69\%$ for ν_μ CC. The probability of misidentifying a primary hadron track as a muon was studied using neutral current (NC) ν_μ interactions and results to be less than 0.36%. Having on average 5 charged hadron tracks per event, this implies a purity in muon identification of almost 99%. Table 4 reports the event classification for CC and NC muon neutrino interactions. 0μ events are those without any muon reconstructed in the final state. Events with one or more muons reconstructed are labelled as 1μ or $n\mu$ events. As it can be seen, 69% of the CC interactions show at least one reconstructed muon while the probability for a NC interaction to be properly classified as 0μ is above 99%.

The estimated muon identification efficiency can be improved not only with a better offline selection, but also moving to a muon system where the scintillating bars of the three most downstream planes in the muon system are replaced by tiles, as foreseen for the extended run configuration.

Electron identification Electrons produced by neutrino scattering are identified by the observation of the electromagnetic shower induced inside the interaction brick.

	% evts CC-DIS	% evts NC-DIS
0μ	31.1	99.6
1μ	67.6	0.27
2μ	1.13	0.06
3μ	0.1	0.03
$> 3\mu$	0.01	0

Table 4: Event classification for CC and NC interactions.

decay channel	ϵ_{ds} (%)	ϵ_{tot} (%)
$\tau \to \mu$	82.5 ± 1.6	49.6 ± 1.8
$\tau \to e$	80.8 ± 1.7	48.4 ± 1.8
$\tau \to h$	80.3 ± 1.0	48.4 ± 1.1
$\tau \to 3h$	89.4 ± 1.5	54.0 ± 1.9

Table 5: Decay search and overall efficiencies for the different τ decay channels

Electromagnetic showers originated by photons are separated from those initiated by electrons thanks to the micrometric accuracy of the nuclear emulsion that is capable of observing the displaced vertex associated with the photon conversion. This procedure is characterized by an efficiency larger than 95%.

The SciFi detector will complement the emulsion detector in the identification of electromagnetic showers and in the electron/π^0 separation, thus achieving an efficiency of about 99%.

Tau identification The selection of the τ lepton candidates is based on purely topological criteria. Once the primary neutrino interaction vertex has been defined, possible secondary vertices, sign of possible short lived particle decays, are searched for. This is done by a decay search procedure: tracks are defined as belonging to a secondary vertex if the impact parameter of the daughter track with respect to the primary vertex is larger than 10 μm. The fraction of events in which the tau lepton decays before the last five emulsion plates is: $\epsilon_{\tau length} = 74.8 \pm 0.7\%$.

The decay search efficiency ϵ_{ds} ranges from 80% to 89% for the different channels as it is summarized in Table 5. The total efficiency ϵ_{tot}, also reported in Table 5, is the combination of geometrical, location and decay search efficiencies: $\epsilon_{tot} = \epsilon_{geom} \cdot \epsilon_{loc} \cdot \epsilon_{\tau length} \cdot \epsilon_{ds}$ and ranges from 48.4% in the $\tau \to h$ decay channel up to 54% in the $\tau \to 3h$ decay channel.

7.2.2 Background in the tau neutrino search

Tau neutrino interactions are identified with the observation of two-vertices events. Hadron re-interactions and charmed particles decays may mimic this topology. The hadronic re-interaction background can however be strongly reduced requiring a single or a three-prong topology and the absence of nuclear fragments up to $\tan\theta = 3$.

Charmed hadrons are produced at a level of a few percent in high energy neutrino and anti-neutrino charged-current interactions [7] via the process reported in Fig. 25. When the

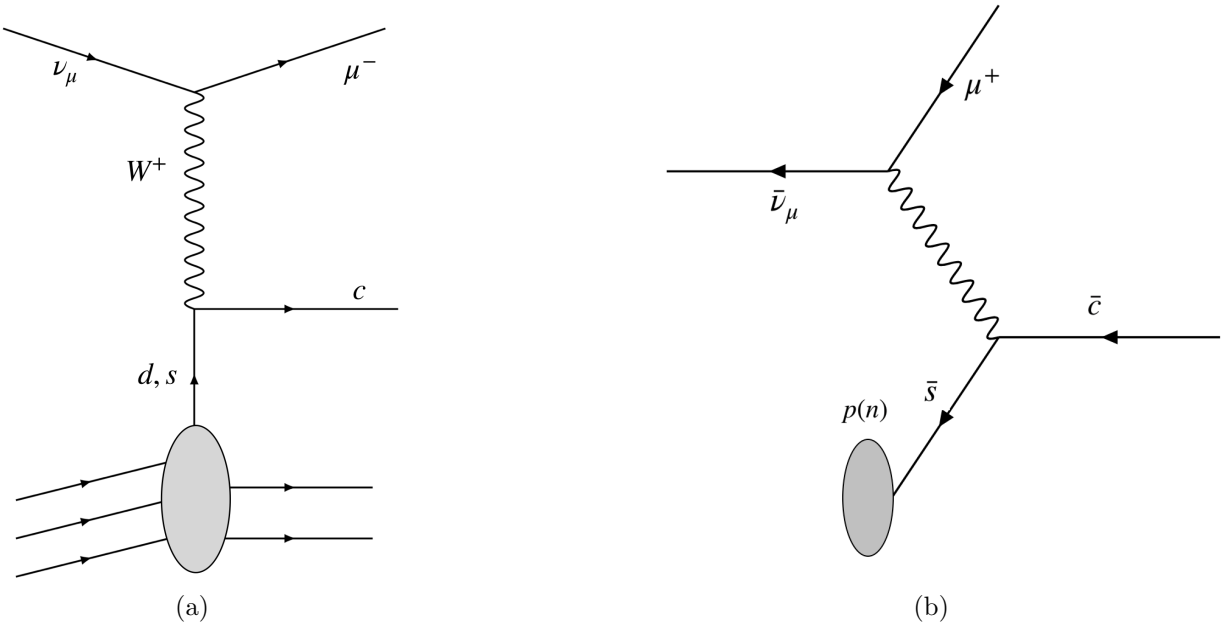

Figure 25: Charm production in neutrino (a) and anti-neutrino (b) charged-current interactions.

lepton produced in the neutrino charged current interaction is not identified, the $\nu_\mu(\bar{\nu}_\mu)$ and $\nu_e(\bar{\nu}_e)$ interaction with subsequent charmed hadron production are the main background to ν_τ searches. The expected charm yields and the corresponding fractions w.r.t. the neutrino charged current interactions are reported in table 6.

Given the muon identification efficiency, the expected number of charmed hadron events induced from ν_μ ($\bar{\nu}_\mu$) is 18. This background can be further reduced with dedicated kinematical analysis [14].

Neutrino flavour	$\langle$E$\rangle$ GeV	Charm CC-DIS Interactions	N_{charm}/N_{CC} (%)
ν_μ	510	64	8.2
ν_e	720	24	9.4
$\bar{\nu}_\mu$	585	31	9.6
$\bar{\nu}_e$	790	15	11.5
TOT		134	9.0

Table 6: (Left column) Expected number of CC-DIS interactions with subsequent charm production for the different neutrino flavours in the assumption that 150 fb^{-1} are collected in the initial detector configuration. (Right column) Fraction with respect to the total number of CC-DIS interactions.

7.2.3 Reconstruction of neutrino energy

We exploit the information of the electronic detectors in both the target region and in the muon identification system. Indeed, the whole detector can be considered as a non-homogeneous calorimeter. The energy of the hadronic jet of the neutrino interaction can be reconstructed as:

$$E_{had}^{rec} = A + B \times N\text{hit}_{\text{SciFi}} + C \times N\text{hit}_{\text{MuFilter}} \tag{1}$$

The values of the parameters A, B and C are in GeV units and are obtained by a gradient descent minimisation algorithm applied to simulated events, with the following cost function:

$$J(A, B, C) = J(\underline{\theta}) = \frac{1}{2m} \sum_{i=1}^{m} (E_{had}^{rec\,(i)} - E_{had}^{true\,(i)})^2 \tag{2}$$

where m is the number of events. The best-fit parameter values are: A = 1.0 GeV, B = 0.5 GeV, C = 0.44 GeV. The resolution on the reconstructed hadronic energy is reported in Fig. 26. The fractional resolution is $\sigma(E_{had}) = (22.3 \pm 0.6)\%$.

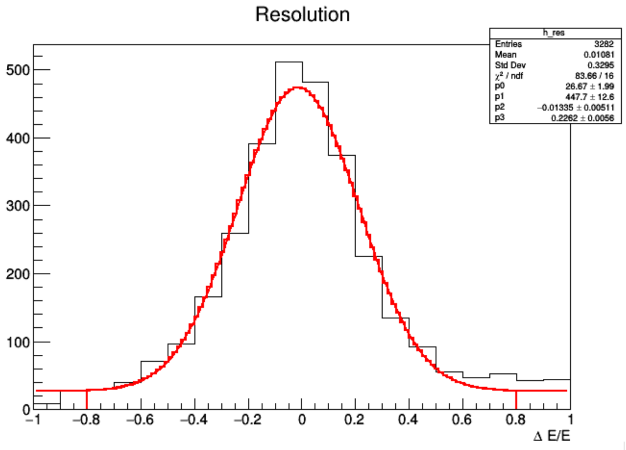

Figure 26: $\Delta E/E$ distribution of the reconstructed hadronic energy.

For ν_μ ($\bar{\nu}_\mu$) charged current interactions, the momentum of the outgoing muon can be estimated by balancing the transverse momentum of the hadronic system. Dedicated algorithms based on multivariate techniques will be used to extract the neutrino energy.

7.3 Light Dark Matter search

The increasing interest in the understanding of the nature of Dark Matter has been lately accompanied by a corresponding effort of the scientific community, both in direct and indirect searches as described in Sec. 1. Complementary approaches such as the direct observation of Dark Matter scattering off electrons have been conceived, as proposed by the SHiP experiment at the CERN SPS [17, 29].

The Scattering and Neutrino Detector here presented is capable of performing model-independent searches for FIPs, thus exploring a large variety of the Beyond Standard Model (BSM) scenarios describing Hidden Portals. Among the most compelling ones, the paradigm of

a Vector Portal which, in a minimal SM extension, reports the production of a vector mediator *Dark Photon* $\mathcal{A}'$ (DP):

$$\mathcal{L}_{\mathcal{A}'} = -\frac{1}{4}F'_{\mu\nu}F'^{\mu\nu} + \frac{m^2_{\mathcal{A}'}}{2}A'^{\mu}A'_{\mu} - \frac{1}{2}\epsilon F'_{\mu\nu}F^{\mu\nu}\,, \tag{3}$$

which is kinetically mixed with the photon field $F^{\mu\nu}$ via the coupling ϵ.

For this study we consider prompt decays of DP into a pair of Light Dark Matter (LDM) candidates χ (i.e. $m_\chi \sim O(1\,\mathrm{GeV/c^2})$ either fermionic or scalar, charged under a new $U'(1)$ symmetry:

$$\mathcal{L}_\chi = g_D\, A'^{\mu} \times \begin{cases} \bar{\psi}_\chi \gamma_\mu \psi_\chi \\ i[(\partial_\mu \phi^\dagger_\chi)\phi_\chi - \phi^\dagger \partial_\mu \phi_\chi] \end{cases} \tag{4}$$

being ψ_χ and ϕ_χ the fermionic and scalar candidates, respectively; the parameter g_D denotes the gauge coupling of the introduced dark sector U'.
In the regime $m_{A'} > 2\,m_\chi$ (invisibly decaying DP) and $\alpha_D = g_D^2/4\,\pi \gg \epsilon\, e$, it is reasonable to assume a short-lived DP with $\mathrm{BF}(A' \to \chi\chi^\dagger) \approx 1$.

At SND, a multitude of processes give rise to the production of DPs and, consequently, LDM particles. In the considered mass range $m_{\mathcal{A}'} \lesssim 1$ GeV, two mechanisms are leading:

- *Meson decays*: DPs abundantly originate from radiative decays of light mesons in

$$\pi^0,\, \eta,\, \eta' \to \gamma\mathcal{A}',$$

$$\omega \to \pi^0\mathcal{A}'\,.$$

- *Bremsstrahlung of protons*: interacting primary protons at the LHC collision point radiate DPs at a very low angular spread.

It is here noted that on-shell production of DPs from prompt-QCD interactions contributes to a negligible extent, thus ignored for this study.

The experimental signature considered in this study is the LDM elastic scattering off the detector atomic electrons:

$$\chi\, e^- \to \chi\, e^-$$

where the recoil electron-induced shower is reconstructed in the target region with high position resolution and angular precision, thanks to its high-granularity. LDM elastic scattering off nuclei and inelastic scattering represent an appealing perspective and are left as subject for future investigation.

Possible backgrounds to this search consist of neutrino interactions where exclusively one charged track, either an electron or positron, is reconstructed at the primary vertex. Different contribution channels have been investigated, namely: neutrino-electron CC/Neutral Current (NC) scattering $\nu_x\, e^- \to \nu_x\, e^-$, exhibiting the same topology of the signal; $\nu_e(\bar{\nu}_e)$ CC Deep Inelastic Scattering (DIS), CC Resonant Scattering (CCRES) and CC Quasi-Elastic Scattering (CCQE) with soft undetectable tracks at the neutrino vertex.

Full Monte Carlo simulations performed by means of the software packages described in Sec. 7.2 for the incoming neutrino flux and by Genie [63] for the neutrino scattering, have shown that the background comes exclusively from CCDIS interactions, given the negligible yield of other sources. Once visibility criteria (Tab. 3) are applied to the tracks produced in

CCDIS interactions, the corresponding yield becomes negligible. Zero background is therefore assumed in the following analysis.

A full MC simulation has been performed also for the signal. LDM candidates have been produced by means of PYTHIA8 [65, 66] and MadDump [67] MC generators, the latter tuned to describe the current detector configuration and model physical parameters: a benchmark scenario is assumed, in which $m_{\mathcal{A}'} = 3\,m_\chi$ and $\alpha_D = 0.1$. We report in Fig. 27 the projected 90% C.L. exclusion limits in the plane (M_χ, $Y = \epsilon^2\alpha_D\left(M_\chi/M_{A'}\right)^4$) for the full data-taking period (150 fb^{-1}), compared to existing constraints.

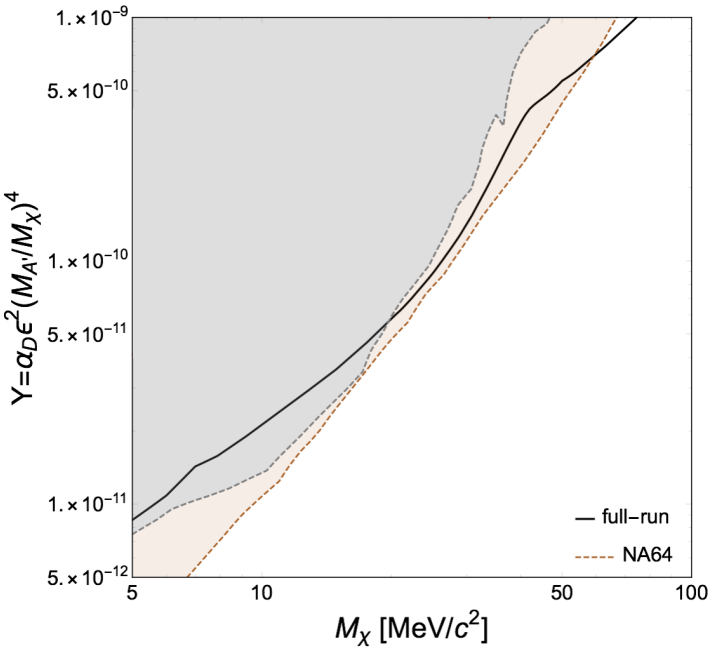

Figure 27: SND 90% C.L. exclusion limits in the 0-background scenario for a LDM candidate χ originated from the prompt decay of a DP $\mathcal{A}'$, assuming as benchmark parameters $m_{\mathcal{A}'} = 3\,m_\chi$ and $\alpha_D = 0.1$.

A complementary approach consists of using the Time Of Flight (TOF) measurement, once the time information is matched to the ECC. With a time resolution of ~ 200 ps, it will be possible to disentangle any FIP scattering process w.r.t. neutrino ones, with a significance which depends on the particle mass. The exploitable phase space of this proposal is shown in terms of sensitivity curves from 1 to 5σ in the plane ($M_{\rm NP}$, $p_{\rm NP}$) in Fig. 28, where $M_{\rm NP}$ and $p_{\rm NP}$ denote the mass and momentum, respectively, of the new physics candidate to be distinguished from ordinary neutrinos. The 1σ contour in Fig. 28 corresponds to a γ factor of about 50, while the 5σ one to a γ factor of about 25.

The physics case can be extended by adding the scattering with nuclei and other possible models.

8 Installation and operation plan

A preliminary schedule for the installation of all the needed services, cross-checked with EN-ACE-OSS and based on the LHC Long Shutdown 2 Planning [68], is reported in Fig. 29.

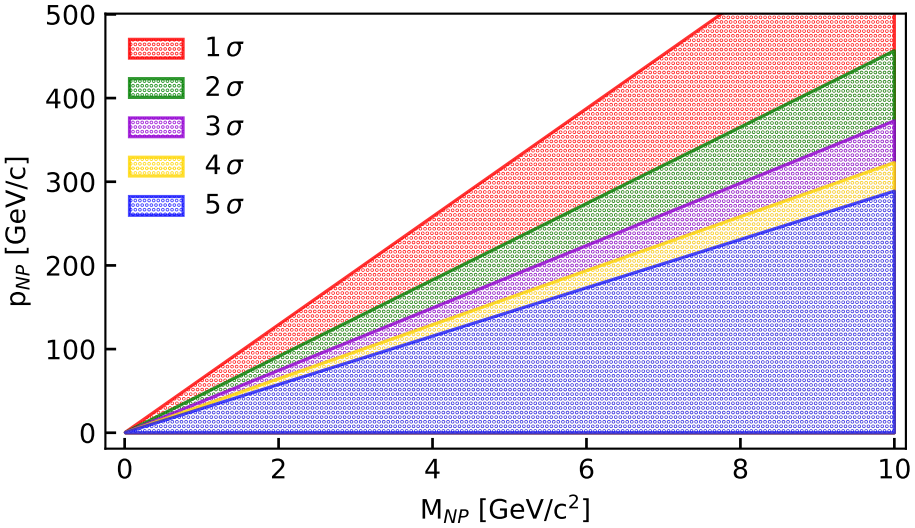

Figure 28: Sensitivity curves for a TOF measurement, illustrated from 1 up to 5σ in the plane ($M_{\rm NP}$, $p_{\rm NP}$) of the New Particle candidates to be detected in the SND, produced assuming a time resolution of $\sim$200 ps.

The duration of each task for the installation of services in TI18 has been estimated and the corresponding CERN groups identified. The timeline reflects preliminary discussions with the different groups. As an example, EN-CV has already pointed out that the chillers need to be previously commissioned on the surface before installing them in the LHC tunnel. Six months are needed from the design phase to their final installation in TI18. Until week number 6 of 2021, the responsible of the LHC machine coordination is EN-ACE-OSS and the available windows for installation are well identified (highlighted in green in the table). Access will also be possible until the end of LS2 to finalise installation and commissioning but it will require careful coordination with BE-OP-LHC as the schedule for the LHC machine tests is not yet fixed.

The installation of services can be completed by February 2021. At the same time, SciFi stations, Scintillator planes and the Veto detector will be ready. Emulsion bricks will be installed at the very last moment, before the LHC machine starts. Additional scintillating bar planes for the muon system will be constructed in the meanwhile.

9 Detector cost

Table 7 gives the estimated cost for the different sub-detectors of the SND.

Nuclear emulsion films will be produced at Nagoya University and by the Slavich Company in Russia. Nagoya University has already produced large surface emulsion films, up to 50×50 cm^2. The Slavich Company is going to install a dedicated production chain for emulsion films required by SND. The total emulsion surface required to instrument the SND target amounts to about 46 m^2. Given the estimated background level, we plan to replace emulsion bricks each 25 fb^{-1}. If we assume to integrate 150 fb^{-1} in 2022, the emulsion target will be replaced six times. A total emulsion surface of about 280 m^2 will be therefore required. The cost reported

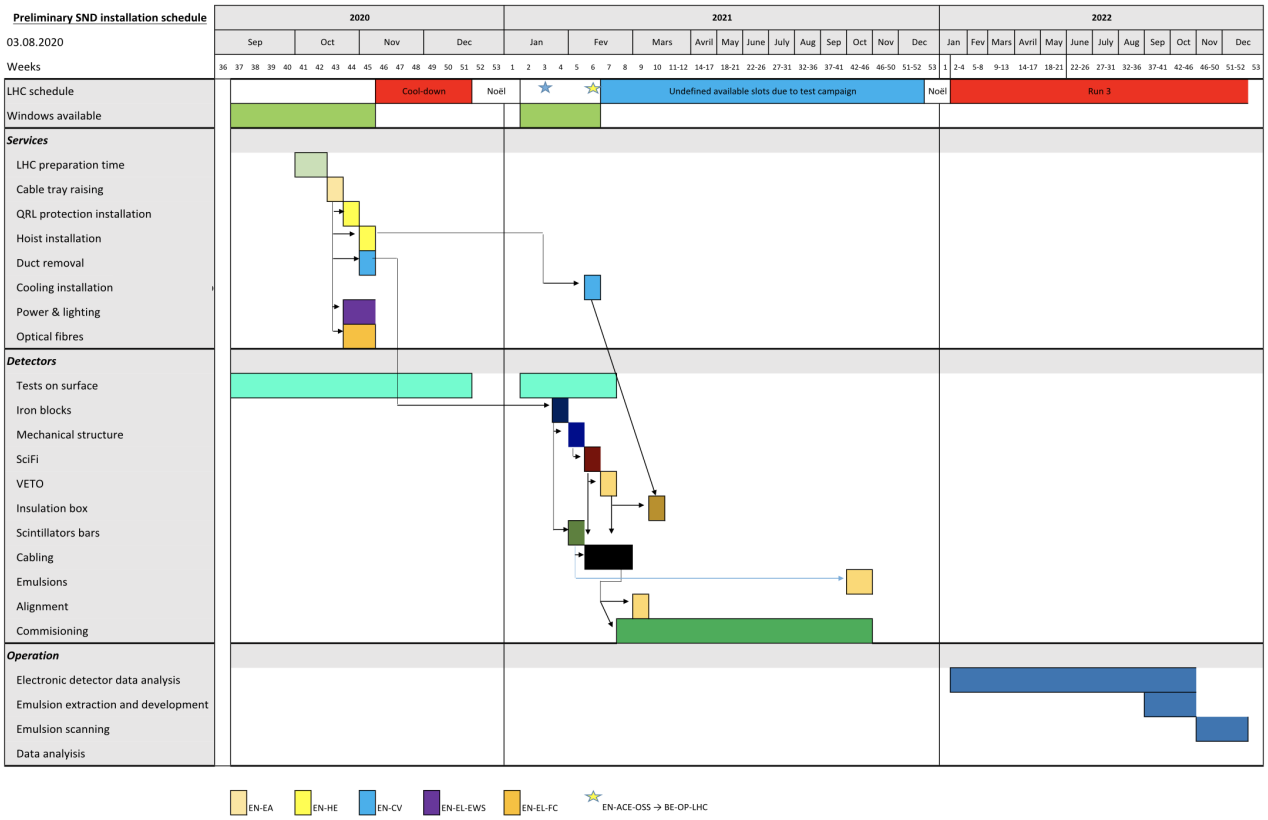

Figure 29: Preliminary plan for the installation of the services and detectors in TI18.

in Table 7 is referring to an average cost of 1kCHF/m^2.
As far as the passive material is concerned, a Chinese firm has already been identified. It is capable of producing Tungsten alloy plates 40×40 cm^2 wide and 1mm thick with the required flatness and roughness. The estimated price is 61 CHF/kg. Given the total target mass of 810 kg and the need to replace the target during the run, 1620 kg will be required, amounting to about 100 kCHF.

Sub-detectors	**Cost**
Nuclear emulsions	280
Tungsten alloy	100
Mechanical structure	25
Veto plane	10
SciFi planes	280
Scintillator planes	160
Total	**855**

Table 7: Cost estimates in kCHF for different components of the SND.

Table 8 reports the estimated cost for infrastructures, as estimated by the different CERN engineering groups.

Component	Cost
Cooling	28
Ventilation	5
Power and lighting	16
Cable tray lowering	6
Networking	20
Transport	25
Survey	20
Total	**120**

Table 8: Cost estimates in kCHF for infrastructures, as estimated by the different CERN engineering groups.

10 Summary

With this paper, the SND Collaboration expresses its interest in the construction and operation of a detector in the TI18 tunnel at the LHC that will, for the first time, measure the process $pp \to \nu X$ in the pseudorapidity region $7.2 < \eta < 8.7$, where neutrinos are mostly produced from charm decays, and search for FIPs in an unexplored domain. The proposed detector is hybrid, combining the nuclear emulsion technology and electronic detectors. This combination results in a very compact and high-performance neutrino detector capable of identifying neutrino interactions of the three flavours and perform searches for neutral massive particles via their scattering on the detector material. The detector is a prototype of the Scattering and Neutrino detector of the SHiP experiment. These measurements will also provide important input to the optimization of neutrino detectors for future experiments at the HL-LHC and at a possible CERN Beam Dump Facility [16].

In 2018 the SHiP Collaboration performed an exposure of an emulsion-based detector to 1.5×10^6 protons at the H4 beamline on the SPS. This exposure aimed at measuring charm production induced by 400 GeV proton interactions in a thick target where the cascade production of charmed hadrons is relevant. This measurement has triggered the development of new reconstruction software in the challenging conditions where proton interactions have to be reconstructed in an environment with a large flux of other particles, with an occupancy in the emulsion up to 5×10^4 particles/cm^2. The results show a good agreement between data and the Monte Carlo simulation both in normalization and in shape, thus demonstrating the feasibility of reconstructing neutrino interactions in the context of the measurement we propose here.

An integration study conducted with all the relevant engineering departments at CERN has not shown any showstopper neither in setting up the relevant services, nor in the detector installation and operation.

With this expression of interest, the SND Collaboration is seeking the approval for a run in 2022 throughout the LHC Run3.

References

[1] **BaBar** Collaboration, J. P. Lees et al., *Evidence for an excess of $\bar{B} \to D^{(*)}\tau^-\bar{\nu}_\tau$ decays*, *Phys. Rev. Lett.* **109** (2012) 101802, [arXiv:1205.5442].

[2] **LHCb** Collaboration, R. Aaij et al., *Test of lepton universality using $B^+ \to K^+\ell^+\ell^-$ decays*, *Phys. Rev. Lett.* **113** (2014) 151601, [arXiv:1406.6482].

[3] **LHCb** Collaboration, R. Aaij et al., *Measurement of the ratio of branching fractions $\mathcal{B}(\bar{B}^0 \to D^{*+}\tau^-\bar{\nu}_\tau)/\mathcal{B}(\bar{B}^0 \to D^{*+}\mu^-\bar{\nu}_\mu)$*, *Phys. Rev. Lett.* **115** (2015), no. 11 111803, [arXiv:1506.08614]. [Erratum: Phys. Rev. Lett.115,no.15,159901(2015)].

[4] **CTEQ** Collaboration, R. Brock et al., *Handbook of perturbative QCD: Version 1.0*, *Rev. Mod. Phys.* **67** (1995) 157.

[5] J. M. Conrad, M. H. Shaevitz, and T. Bolton, *Precision measurements with high-energy neutrino beams*, *Rev. Mod. Phys.* **70** (1998) 1341, [hep-ex/9707015].

[6] J. A. Formaggio and G. P. Zeller, *From eV to EeV: Neutrino Cross Sections Across Energy Scales*, *Rev. Mod. Phys.* **84** (2012) 1307, [arXiv:1305.7513].

[7] G. De Lellis, P. Migliozzi, and P. Santorelli, *Charm physics with neutrinos*, *Phys. Rept.* **399** (2004) 227. [Erratum: Phys. Rept.411,323(2005)].

[8] D. Marfatia, D. W. McKay, and T. J. Weiler, *New physics with ultra-high-energy neutrinos*, *Phys. Lett. B* **748** (2015) 113, [arXiv:1502.06337].

[9] C. A. Argüelles et al., *White Paper on New Opportunities at the Next-Generation Neutrino Experiments (Part 1: BSM Neutrino Physics and Dark Matter)*, [arXiv:1907.08311].

[10] M. Ackermann et al., *Astrophysics Uniquely Enabled by Observations of High-Energy Cosmic Neutrinos*, *Bull. Am. Astron. Soc.* **51** (2019) 185, [arXiv:1903.04334].

[11] **IceCube** Collaboration, M. G. Aartsen et al., *Measurement of the multi-TeV neutrino cross section with IceCube using Earth absorption*, *Nature* **551** (2017) 596, [arXiv:1711.08119].

[12] **DONuT** Collaboration, K. Kodama et al., *Final tau-neutrino results from the DONuT experiment*, *Phys. Rev. D* **78** (2008) 052002, [arXiv:0711.0728].

[13] R. Acquafredda et al., *The OPERA experiment in the CERN to Gran Sasso neutrino beam*, *JINST* **4** (2009) P04018.

[14] **OPERA** Collaboration, N. Agafonova et al., *Final Results of the OPERA Experiment on ν_τ Appearance in the CNGS Neutrino Beam*, *Phys. Rev. Lett.* **120** (2018), no. 21 211801, [arXiv:1804.04912]. [Erratum: Phys. Rev. Lett.121,no.13,139901(2018)].

[15] **OPERA** Collaboration, N. Agafonova et al., *Final results of the search for $\nu_\mu \to \nu_e$ oscillations with the OPERA detector in the CNGS beam*, *JHEP* **06** (2018) 151, [arXiv:1803.11400].

[16] **SHiP** Collaboration, M. Anelli et al., *A facility to Search for Hidden Particles (SHiP) at the CERN SPS*, [arXiv:1504.04956].

[17] S. Alekhin et al., *A facility to Search for Hidden Particles at the CERN SPS: the SHiP physics case*, *Rept. Prog. Phys.* **79** (2016), no. 12 124201, [arXiv:1504.04855].

[18] N. Beni et al., *Physics Potential of an Experiment using LHC Neutrinos*, *J. Phys. G* **46** (2019), no. 11 115008, [arXiv:1903.06564].

[19] **XSEN** Collaboration, N. Beni et al., *XSEN: a νN Cross Section Measurement using High Energy Neutrinos from pp collisions at the LHC*, [arXiv:1910.11340]. CERN-LHCC-2019-014 / LHCC-I-033.

[20] N. Beni et al., "Further studies on the physics potential of an experiment using LHC neutrinos." https://iopscience.iop.org/article/10.1088/1361-6471/aba7ad, accepted for publication on J. Phys. G (2020). [arXiv:2004.07828].

[21] R. K. Ellis et al., *Physics Briefing Book*, [arXiv:1910.11775].

[22] **CRESST** Collaboration, A. H. Abdelhameed et al., *First results from the CRESST-III low-mass dark matter program*, *Phys. Rev. D* **100** (2019), no. 10 102002, [arXiv:1904.00498].

[23] **SuperCDMS** Collaboration, R. Agnese et al., *Projected Sensitivity of the SuperCDMS SNOLAB experiment*, *Phys. Rev. D* **95** (2017), no. 8 082002, [arXiv:1610.00006].

[24] **LDMX** Collaboration, T. Åkesson et al., *Light Dark Matter eXperiment (LDMX)*, [arXiv:1808.05219].

[25] J. Beacham et al., *Physics Beyond Colliders at CERN: Beyond the Standard Model Working Group Report*, *J. Phys. G* **47** (2020), no. 1 010501, [arXiv:1901.09966].

[26] K. Bondarenko et al., *Direct detection and complementary constraints for sub-GeV dark matter*, [arXiv:1909.08632].

[27] **Belle-II** Collaboration, W. Altmannshofer et al., *The Belle II Physics Book*, [arXiv:1808.10567].

[28] D. Banerjee et al., *Dark matter search in missing energy events with NA64*, *Phys. Rev. Lett.* **123** (2019), no. 12 121801, [arXiv:1906.00176].

[29] **SHiP** Collaboration, C. Ahdida et al., *SHiP Experiment - Progress Report*, Scientific Committee Paper CERN-SPSC-2019-010. SPSC-SR-248, CERN, https://cds.cern.ch/record/2654870, Jan, 2019.

[30] A. Bhattacharya, R. Enberg, Y. S. Jeong, C. S. Kim, M. H. Reno, I. Sarcevic, and A. Stasto, *Prompt atmospheric neutrino fluxes: perturbative QCD models and nuclear effects*, *JHEP* **11** (2016) 167, [arXiv:1607.00193].

[31] **FASER** Collaboration, A. Ariga et al., *FASER: ForwArd Search ExpeRiment at the LHC*, [arXiv:1901.04468].

[32] **FASER** Collaboration, H. Abreu et al., *Detecting and Studying High-Energy Collider Neutrinos with FASER at the LHC*, *Eur. Phys. J. C* **80** (2020), no. 1 61, [arXiv:1908.02310].

[33] S. Roesler, R. Engel, and J. Ranft, *The Monte Carlo event generator DPMJET-III*, in *Advanced Monte Carlo for radiation physics, particle transport simulation and applications. Proceedings, Conference, MC2000, Lisbon, Portugal, October 23-26, 2000*, p. 1033, 2000. [hep-ph/0012252].

[34] A. Ferrari, P. R. Sala, A. Fasso, and J. Ranft, *FLUKA: A multi-particle transport code (Program version 2005)*, Tech. Rep. CERN-2005-010, SLAC-R-773, INFN-TC-05-11, 2005.

[35] T. T. Böhlen, F. Cerutti, M. P. W. Chin, A. Fassò, A. Ferrari, P. G. Ortega, A. Mairani, P. R. Sala, G. Smirnov, and V. Vlachoudis, *The FLUKA Code: Developments and Challenges for High Energy and Medical Applications*, *Nucl. Data Sheets* **120** (2014) 211.

[36] **OPERA** Collaboration, N. Agafonova et al., *Observation of a first ν_τ candidate in the OPERA experiment in the CNGS beam*, *Phys. Lett. B* **691** (2010) 138, [arXiv:1006.1623].

[37] **OPERA** Collaboration, N. Agafonova et al., *Search for $\nu_\mu \to \nu_e$ oscillations with the OPERA experiment in the CNGS beam*, *JHEP* **07** (2013) 004, [arXiv:1303.3953]. [Addendum: JHEP07,085(2013)].

[38] **OPERA** Collaboration, N. Agafonova et al., *Evidence for $\nu_\mu \to \nu_\tau$ appearance in the CNGS neutrino beam with the OPERA experiment*, *Phys. Rev.* **D89** (2014), no. 5 051102, [arXiv:1401.2079].

[39] E. Delagnes et al., *The SAMPIC Waveform and Time to Digital Converter*, in *2014 IEEE Nuclear Science Symposium and Medical Imaging Conference (2014 NSS/MIC)*, (Seattle, United States), 2014. Sce Electronique.

[40] C. Betancourt et al., *Application of large area SiPMs for the readout of a plastic scintillator based timing detector*, *JINST* **12** (2017), no. 11 P11023, [arXiv:1709.08972].

[41] H. P. Eckert, *The Mu3e Tile Detector*. PhD thesis, U. Heidelberg (main), 2015.

[42] A. Korzenev et al., *Plastic scintillator detector with the readout based on an array of large-area SiPMs for the ND280/T2K upgrade and SHiP experiments*, in *International Workshop on New Photon Detectors (PD18) Tokyo, Japan, November 27-29, 2018*, 2019. [arXiv:1901.07785].

[43] **OPERA** Collaboration, N. Agafonova et al., *Procedure for short-lived particle detection in the OPERA experiment and its application to charm decays*, *Eur. Phys. J. C* **74** (2014), no. 8 2986, [arXiv:1404.4357].

[44] L. Arrabito et al., *Hardware performance of a scanning system for high speed analysis of nuclear emulsions*, *Nucl. Instrum. Meth. A* **568** (2006) 578, [physics/0604043].

[45] N. Armenise et al., *High-speed particle tracking in nuclear emulsion by last-generation automatic microscopes*, *Nucl. Instrum. Meth. A* **551** (2005) 261.

[46] A. Alexandrov et al., *A new fast scanning system for the measurement of large angle tracks in nuclear emulsions*, *JINST* **10** (2015), no. 11 P11006.

[47] A. Alexandrov et al., *A new generation scanning system for the high-speed analysis of nuclear emulsions*, *JINST* **11** (2016), no. 06 P06002.

[48] A. Alexandrov et al., *The Continuous Motion Technique for a New Generation of Scanning Systems*, *Sci. Rep.* **7** (2017), no. 1 7310.

[49] A. Alexandrov et al., *A Novel Optical Scanning Technique with an Inclined Focusing Plane*, *Sci. Rep.* **9** (2019), no. 1 2870.

[50] **LHCb** Collaboration, *LHCb Tracker Upgrade Technical Design Report*, Report CERN-LHCC-2014-001. LHCB-TDR-015, http://cds.cern.ch/record/1647400, 2014.

[51] **SHiP** Collaboration, *Measurement of associated charm production induced by 400 GeV/c protons*, Scientific Committee Paper CERN-SPSC-2017-033, SPSC-EOI-017, http://cds.cern.ch/record/2286844, 2017.

[52] T. Harion et al., *STiC — a mixed mode silicon photomultiplier readout ASIC for time-of-flight applications*, *JINST* **9** (2014), no. 02 C02003.

[53] M. Chadeeva, *CALICE highly granular calorimeters: imaging properties for hadronic shower analysis*, *JINST* **15** (2020), no. 07 C07014.

[54] F. Delsaux et al., *FASER-UJ12-PROTECTION MACHINE LHC*, EDMS LHCQRMPI0001 v.0, CERN, https://edms.cern.ch/document/2218714/0, 20 Aug, 2019.

[55] M. Brucoli, *Report on the Radiation on Electronics measurements for FASER experiment*, EDMS 2080681 v.1, CERN, https://edms.cern.ch/document/2080681/1, 24 Jan, 2019.

[56] C. Galliard, *Alignment aimants quadrupole ensemble verin*, EDMS SPS8014006040-vAA, CERN, https://edms.cern.ch/document/277014/AA, 01 Nov, 1973.

[57] K. Morishima and T. Nakano, *Development of a new automatic nuclear emulsion scanning system, S-UTS, with continuous 3D tomographic image read-out*, *JINST* **5** (2010) P04011.

[58] L. Arrabito et al., *Track reconstruction in the emulsion-lead target of the OPERA experiment using the ESS microscope*, *JINST* **2** (2007) P05004, [arXiv:0705.3102].

[59] N. Armenise et al., *High-speed particle tracking in nuclear emulsion by last-generation automatic microscopes*, *Nucl. Instrum. Meth. A* **551** (2005) 261.

[60] **SHiP** Collaboration, "Heavy Flavour Cascade Production in a Beam Dump." https://cds.cern.ch/record/2115534, Dec, 2015. CERN-SHiP-NOTE-2015-009.

[61] M. Al-Turany, D. Bertini, R. Karabowicz, D. Kresan, P. Malzacher, T. Stockmanns, and F. Uhlig, *The FairRoot framework*, *J. Phys. Conf. Ser.* **396** (2012) 022001.

[62] V. Boccone et al., *Beam-machine interaction at the cern lhc*, *Nuclear Data Sheets* **120** (2014) 215 – 218.

[63] C. Andreopoulos et al., *The GENIE Neutrino Monte Carlo Generator*, *Nucl. Instrum. Meth. A* **614** (2010) 87, [arXiv:0905.2517].

[64] **GEANT4** Collaboration, S. Agostinelli et al., *GEANT4: A Simulation toolkit*, *Nucl. Instrum. Meth. A* **506** (2003) 250.

[65] T. Sjöstrand, S. Mrenna, and P. Z. Skands, *A Brief Introduction to PYTHIA 8.1*, *Comput. Phys. Commun.* **178** (2008) 852, [arXiv:0710.3820].

[66] T. Sjöstrand, S. Ask, J. R. Christiansen, R. Corke, N. Desai, P. Ilten, S. Mrenna, S. Prestel, C. O. Rasmussen, and P. Z. Skands, *An Introduction to PYTHIA 8.2*, *Comput. Phys. Commun.* **191** (2015) 159, [arXiv:1410.3012].

[67] L. Buonocore, C. Frugiuele, F. Maltoni, O. Mattelaer, and F. Tramontano, *Event generation for beam dump experiments*, *JHEP* **05** (2019) 028, [arXiv:1812.06771].

[68] M. Alcaide et al., *LHC Long Shutdown 2 Planning*, EDMS LHC-PM-MS-0018 v.2.3, CERN, https://edms.cern.ch/document/1817804/2.3, 2020.